Title

DNMT3A Haploinsufficiency Transforms FLT3ITD Myeloproliferative Disease into a Rapid, Spontaneous, and Fully Penetrant Acute Myeloid Leukemia

Journal

Cancer Discovery, 6(5)

ISSN

2159-8274

Authors

Meyer, Sara E
Qin, Tingting
Muench, David E
et al.

Publication Date

2016-05-01

DOI

10.1158/2159-8290.cd-16-0008

Peer reviewed

HHS Public Access

Author manuscript

Cancer Discov. Author manuscript; available in PMC 2017 May 01.

Published in final edited form as:

Cancer Discov. 2016 May ; 6(5): 501–515. doi:10.1158/2159-8290.CD-16-0008.

Dnmt3a haploinsufficiency transforms Flt3-ITD myeloproliferative disease into a rapid, spontaneous, and fully-penetrant acute myeloid leukemia

Sara E. Meyer[1], **Tingting Qin**[2], **David E. Muench**[1], **Kohei Masuda**[1], **Meenakshi Venkatasubramanian**[3], **Emily Orr**[1], **Lauren Suarez**[4], **Steven D. Gore**[5], **Ruud Delwel**[6], **Elisabeth Paietta**[7], **Martin S. Tallman**[8], **Hugo Fernandez**[9], **Ari Melnick**[10], **Michelle M. Le Beau**[11], **Scott Kogan**[12], **Nathan Salomonis**[3], **Maria E. Figueroa**[2,*], and **H. Leighton Grimes**[1,13,*]

[1]Division of Immunobiology, Cincinnati Children's Hospital Medical Center, Cincinnati, Ohio, USA [2]Department of Pathology, University of Michigan Medical School, Ann Arbor, Michigan, USA [3]Division of Biomedical Informatics, Cincinnati Children's Hospital Medical Center, Cincinnati, Ohio, USA [4]Department of Oncology, The Sidney Kimmel Comprehensive Cancer Center, Johns Hopkins University School of Medicine, Baltimore, Maryland, USA [5]Division of Hematologic Malignancies, Yale Cancer Center, Yale School of medicine, New Haven, Connecticut, USA [6]Department of Hematology, and Clinical Trial Center, Erasmus University Medical Center, Rotterdam, The Netherlands [7]Division of Hemato-Oncology, Department of Medicine (Oncology), Albert Einstein College of Medicine/Montefiore Medical Center, Bronx, New York, USA [8]Leukemia Service, Memorial Sloan Kettering Cancer Center, New York, New York, USA [9]Blood and Marrow Transplantation, Moffitt Cancer Center, Oncologic Sciences, College of Medicine at University of South Florida, Florida, USA [10]Department of Medicine, Hematology Oncology Division, Cornell, New York, USA [11]Section of Hematology/Oncology, and the Comprehensive Cancer Center, University of Chicago, Chicago, Illinois, USA [12]Department of Laboratory Medicine & Helen Diller Family Comprehensive Cancer Center, University of California San Francisco, San Francisco, California, USA [13]Division of Experimental Hematology and Cancer Biology, Cincinnati Children's Hospital Medical Center, Cincinnati, Ohio, USA

Abstract

Cytogenetically normal acute myeloid leukemia (CN-AML) represents nearly 50% of human AML. Co-occurring mutations in the *de novo* DNA methyltransferase *DNMT3A* and the *FMS related tyrosine kinase 3 FLT3* are common in CN-AML and confer a poorer prognosis. We

[*]co-corresponding authorship: H. Leighton Grimes, PhD, Division of Immunobiology, Cincinnati Children's Hospital Medical Center, 3333 Burnet Ave MLC 7038, Cincinnati, OH 45229, Tel: 513.636.6089, Fax: 513.636.5355, lee.grimes@cchmc.org. Maria E. Figueroa, MD, Department of Pathology, University of Michigan, 109 Zina Pitcher Place, BSRB 2019, Ann Arbor, MI 48109-2200, Tel: 734-763-1865, marfigue@med.umich.edu.

Conflict of Interest Statement

The authors have no conflicts to disclose.

Accession Numbers

RNA sequencing (GEO accession GSE77849) and ERRBS data (GEO accession GSE77026) can be accessed in the Gene Expression Omnibus.

demonstrate that mice with *Flt3*-internal-tandem duplication (*Flt3*^{ITD}) and inducible deletion of *Dnmt3a* spontaneously develop a rapidly-lethal, completely-penetrant, and transplantable AML of normal karyotype. AML cells retain a single *Dnmt3a* floxed allele, revealing the oncogenic potential of *Dnmt3a* haploinsufficiency. *FLT3*-ITD/*DNMT3A*-mutant primary human and murine AML exhibit a similar pattern of global DNA methylation associated with changes in the expression of nearby genes. In the murine model, rescuing *DNMT3A* expression was accompanied by DNA re-methylation and loss of clonogenic potential, suggesting that Dnmt3a-mutant oncogenic effects are reversible. Dissection of the cellular architecture of the AML model using single-cell assays identified clonogenic subpopulations that express genes sensitive to the methylation of nearby genomic loci, and responsive to Dnmt3a levels. Thus, *Dnmt3a* haploinsufficiency transforms *Flt3*^{ITD} myeloproliferative disease by modulating methylation-sensitive gene expression within a clonogenic AML subpopulation.

Keywords

Epigenetics; Acute Myeloid Leukemia; Myeloproliferative Neoplasm; Dnmt3a; Flt3

Introduction

FLT3 is one of the most frequently mutated genes in cytogenetically normal acute myeloid leukemia (CN-AML), affecting 37% of cases (1–3). *FLT3* internal tandem duplication (ITD) mutations are associated with a worse overall survival, and constitute an independent prognostic factor for relapse and poor outcome in AML (4–7). Recently, recurrent mutations were found in the epigenetic regulators *DNMT3A* and *TET2* (2, 3, 8–11). It is now recognized that DNA methyltransferase *DNMT3A* is one of the more commonly mutated genes in AML, affecting 23% of cases, and is associated with an unfavorable prognosis (3, 12–14). Intriguingly, 36–44% of *FLT3* mutant AML patients also carry *DNMT3A* mutations. Furthermore, the co-occurrence of *DNMT3A* and *FLT3* mutants changes the risk classification to a poorer prognosis (3, 12, 13).

The mammalian DNA methyltransferases DNMT1, DNMT3A and DNMT3B methylate the cytosine residue at 5 position (5mC) in 5′-C-phosphate-G-3′ (CpG) dinucleotides. Methylation of CpG sites at promoter-associated CpG islands is thought to silence expression of neighboring genes. In addition, methylation of CpG dinucleotides can also occur at the gene body or intergenic regions, where it's role in gene regulation is less clear (15). Different molecular subtypes of CN-AML have highly divergent DNA methylation and transcription profiles (16, 17). Recurring missense mutations in *DNMT3A* identified in CN-AML act as loss-of-function or dominant negatives, significantly reducing the methyltransferase activity of DNMT3A by approximately 80% (11, 18, 19). While the mechanisms of DNMT3A action in the pathogenesis of AML are still unclear, studies on stem cells demonstrate essential roles for all DNMT proteins. DNMT1 is required to maintain global DNA methylation through successive rounds of cell division, whereas the *de novo* methyltransferases DNMT3A and DNMT3B are required for mouse embryonic development (20). Serial transplantation of *Dnmt3a* knockout hematopoietic stem/progenitor cells (HSPC) results in impaired differentiation, enhanced proliferation, and differential

methylation of distinct genetic loci resulting in upregulation of stemness genes and proto-oncogenes, and downregulation of differentiation genes (21). Despite this, *Dnmt3a* knockout HSPC reconstituted mice do not develop AML.

FLT3-ITD mutant receptors undergo ligand-independent receptor dimerization, auto-phosphorylation, and constitutive activation (22–24). Mouse knock-in and human cell models of FLT3-ITD demonstrate FLT3 mutant receptors promote aberrant cell proliferation through activation of Stat5, Akt/Erk, and c-Myc pathways, and impair differentiation by altering expression of myeloid transcription factors such as CEBPα (25–32). Despite the high frequency of FLT3 mutations in AML, murine models of $Flt3^{ITD}$ develop a mixture of myeloid and lymphoid neoplasms either as a single mutation or in combination with other oncogenic events such as MLL partial tandem duplication (Mll^{PTD}) (25, 27, 33–35). Importantly, $Flt3^{ITD}$ mice do not progress to leukemia, thus other cooperating mutations must be required for development of AML.

Results

To test whether *Flt3* and *Dnmt3a* mutations cooperate to initiate leukemogenesis we bred mice to combine $Flt3^{ITD}$ knock-in and homozygous *Dnmt3a* floxed alleles ($Dnmt3a^{fl/fl}$) (Fig. 1A) with *Mx1-Cre* (*MxCre*). We find that $Flt3^{+/ITD}$;$Dnmt3a^{fl/fl}$ *MxCre* mice (with one mutant *Flt3* allele) have a long median survival of 227 days and exhibited splenomegaly (Supplementary Fig. S1A). Control $Flt3^{+/ITD}$;$Dnmt3a^{fl/fl}$ mice did not die in this time period. Conversely, doubling the number of $Flt3^{ITD}$ alleles significantly shortened survival with a median of 43 days after birth (Fig. 1B left and lower table). All $Flt3^{ITD/ITD}$;$Dnmt3a^{fl/fl}$ *MxCre* mice exhibited splenomegaly (Fig. 1B right), and were moribund by 60 days. Secondary and tertiary transplantation of $Flt3^{ITD/ITD}Dnmt3a^{fl/fl}$ *MxCre* splenocytes resulted in lethality, albeit with delayed latency (Supplementary Fig. S1B and data not shown). Because the disease occurred spontaneously (pIpC induction of *Mx1-Cre* expression was not required), we examined the $Dnmt3a^{fl/fl}$ alleles (Fig. 1C). As expected, tail DNA from two week-old $Flt3^{ITD/ITD}$;$Dnmt3a^{fl/fl}$ *MxCre* mice showed amplification of *loxP*-flanked *Dnmt3a* exon 18 (Fig. 1C, “floxed” indicates no recombination; “deleted” indicates recombination). However, total or fractionated c-Kit^+ (CD117) stem/progenitor enriched splenocytes from $Flt3^{ITD/ITD}$;$Dnmt3a^{fl/fl}$ *MxCre de novo* or secondary transplant recipients demonstrated both floxed and deleted *Dnmt3a* alleles (Fig. 1C). In addition, we plated c-Kit^+ $Flt3^{ITD/ITD}$;$Dnmt3a^{fl/fl}$ *MxCre* hematopoietic cells in methylcellulose, isolated DNA from individual colonies, and then analyzed floxed *Dnmt3a* alleles. Of 77 colonies analyzed, 28 lacked detectable floxed alleles (36%), thus the majority of cells spontaneously deleted only one allele of *Dnmt3a* (Supplementary Fig. S1C). In agreement with this, the mRNA from c-Kit^+ cells from $Flt3^{ITD/ITD}$;$Dnmt3a^{fl/fl}$ *MxCre* mice showed sporadic low-level expression of *Cre*, and approximately 50% reduction in *Dnmt3a* expression (Fig. 1D). These data suggest that sporadic *MxCre* expression leads to excision of floxed *Dnmt3a* alleles, and that $Flt3^{ITD/ITD}$ cells with a single *Dnmt3a* allele may have a selective advantage.

Examination of the blood, bone marrow, spleen and liver of moribund $Flt3^{ITD/ITD}$;$Dnmt3a^{fl/fl}$ *MxCre* mice demonstrated pathologic features of myeloid leukemia.

The peripheral blood was notable for anemia and for leukocytosis of neutrophilic and monocytic cells, including immature forms (Supplementary Table S1 and data not shown). Bone marrow contained immature forms/blasts that were greater than 20% of nucleated cells along with numerous intermediate myeloid forms (i.e. non-blast myelomonocytic cells that have not differentiated sufficiently to be distinguished into monocytic or neutrophilic cells by morphology) (36). Similar to *Flt3*$^{ITD/ITD}$*;Dnmt3a*$^{fl/fl}$ mice there was a marked decrease in erythroid and lymphoid cells relative to wild-type (WT) marrow (Fig. 1E, top two rows). The massively enlarged spleens of the *Flt3*$^{ITD/ITD}$*;Dnmt3a*$^{fl/fl}$ *MxCre* mice contained areas of predominantly immature cells (similar to those seen in the marrow), but most of the red pulp contained a mix of maturing neutrophilic, monocytic, erythroid and megakaryocytic cells (Fig. 1E, third row). Concordant with the morphology, flow cytometric immunophenotyping of erythroid-depleted bone marrows and spleens of *Flt3*$^{ITD/ITD}$*;Dnmt3a*$^{fl/fl}$ *MxCre* mice showed decreased lymphocytes (data not shown and Supplementary Fig. S1D) and increased monocytic cells (CD11b^{+}, Gr1^{-}, B220^{-}) in comparison to WT mice, and increased immature cells (Lin^{-}c-Kit^{+}, abbreviated LK) in comparison to *Flt3*$^{ITD/ITD}$*;Dnmt3a*$^{fl/fl}$ mice (Supplementary Fig. S1E–I, Supplementary Table S2). In contrast to the *Flt3*$^{ITD/ITD}$*;Dnmt3a*$^{fl/fl}$ mice, myelomonocytic cells aggressively invaded the perivascular and sinusoidal regions of the liver (Fig. 1E, fourth row). These pathologic findings are indicative of myelomonocytic leukemia. The presence of greater than 20% immature forms/blasts in the bone marrows of *Flt3*$^{ITD/ITD}$*;Dnmt3a*$^{fl/fl}$ *MxCre* mice in combination with the rapid lethality observed in the primary animals warranted a diagnosis of acute leukemia (36). In agreement with previous reports, *Flt3*$^{ITD/ITD}$*;Dnmt3a*$^{fl/fl}$ control mice (Fig. 1E, second column) showed expansion of both mature and immature myeloid cells, consistent with myeloproliferative neoplasm (MPN) (27). According to these diagnoses, we hereon refer to *Flt3*$^{ITD/ITD}$*;Dnmt3a*$^{fl/fl}$ mice as MPN and *Flt3*$^{ITD/ITD}$*;Dnmt3a*$^{fl/fl}$ *MxCre* mice as AML.

To assess the ability of the leukemic cell populations to give rise to colony forming units (CFUs), we seeded purified c-Kit^{+} and c-Kit^{-} cells from moribund mice into methylcellulose. The c-Kit^{+} fraction from several different donor mice gave rise to significantly more colonies than the c-Kit^{-} fraction, compatible with c-Kit^{+} leukemic blasts (Supplementary Fig. S1J). Moreover, c-Kit^{+} splenocytes from AML mice had significantly increased colony forming ability compared to c-Kit^{+} splenocytes from MPN mice (Fig. 1F). No differences in colony morphologies or numbers between c-Kit^{+} bone marrow and c-Kit^{+} splenocytes from AML mice were observed (data not shown). We conclude that loss of one *Dnmt3a* allele is sufficient to increase the clonogenic potential of *Flt3*^{ITD} myeloid progenitors.

Since *FLT3*-ITD and *DNMT3A* mutations are most common in AML patients with normal karyotype, we performed spectral karyotyping analyses on bone marrow from five independent murine AML (Fig. 1G). Four of five AMLs exhibited normal karyotypes and one had a small clone with loss of the Y chromosome (39,X, -Y[4]/40,XY[16]). Note that loss of the Y chromosome is observed in both malignant and non-malignant states, and is not considered to be a driver mutation. Like their human counterparts with similar mutations, the murine model tumors are cytogenetically normal AML.

Since the murine AML express less *Dnmt3a* mRNA, we next investigated whether our model recapitulated the epigenetic abnormalities seen in human *DNMT3A*-mutant AML, where activity of the enzyme is compromised due to the dominant-negative nature of the mutation (11, 18, 19). Using Enhanced Reduced Representation Bisulfite Sequencing (ERRBS) (37), we derived the disease-specific DNA-methylation profiles in both human and murine AML with similar mutation profiles. First, we compared primary human AML carrying both *FLT3*-ITD and *DNMT3A*-mutations (*FLT3*-ITD/*DNMT3A*-mut) versus *FLT3*-ITD AML lacking mutations in *DNMT3A* (*FLT3*-ITD/*DNMT3A*-wt). To ensure that the DNA methylation differences we observed could only be explained by the *DNMT3A* status, patients with mutations in other genes related to the DNA methylation pathway (*TET2, IDH1* and *IDH2*) were excluded from both groups. Differentially methylated regions (DMR) with an FDR<10% and a mean methylation difference ≥25% were identified using a beta-binomial model. Patients with *FLT3*-ITD/*DNMT3A*-mut presented with a predominantly hypomethylated profile compared to *FLT3*-ITD/*DNMT3A*-wt cases (95.9% hypomethylated regions of 25,746 total DMR). These differentially methylated regions in *FLT3*-ITD/*DNMT3A*-mut AML were significantly enriched at CpG shores (22% of DMRs at CpG shores versus 15% in background, $p<2.2x10^{-16}$) and enhancer regions (33% of DMRs at intragenic enhancers versus 19% in background, $p<2.2x10^{-16}$ and 24% at intergenic enhancers versus 15% in background, $p<2.2x10^{-16}$) (Fig. 2A–C, Supplementary Table S3). Next, we compared the murine AML versus MPN c-Kit^{+} splenocytes. Similar to our findings in human AML, *Dnmt3a* loss was associated with predominance of hypomethylation (80.7% hypomethylated regions of 503 total DMR) with enrichment of DMRs at enhancer regions (9% of DMRs at intragenic enhancers versus 3% background, $p=1.519x10^{-10}$ and 6% of DMRs at intergenic enhancers versus 2% background, $p=6.005x10^{-7}$) (Fig. 2D–F, Supplementary Table S3). Importantly, we found that 61.8% of the DMR identified in the murine models (*Flt3*$^{ITD/ITD}$*;Dnmt3a*$^{fl/fl}$ *MxCre* AML versus *Flt3*$^{ITD/ITD}$*;Dnmt3a*$^{fl/fl}$ MPN) overlapped with the human *FLT3*-ITD/*DNMT3A*-mutant signature.

We next determined the DNA methylation status of these DMRs in normal human and murine HSPC. We note that the methylation of a subset of DMR is similar in both *DNMA3A*-mut leukemic and normal human hematopoietic stem cells (HSC) or murine AML and Lin^{-}Sca-1^{+}c-Kit^{+} (LSK) cells (Fig. 2B, 2E; “HSPC-like” DMRs) (Supplementary Table S3), suggesting that *Dnmt3a*-mutant AML cells lack adequate Dnmt3a levels to mediate normal differentiation-associated methylation of these genomic loci. In contrast, other DMR were not found in normal progenitors, and instead displayed methylation patterns unique to the *DNMT3A*-mutant human and mouse AMLs (Fig. 2B, 2E; “AML-unique” DMRs) (Supplementary Table S3). These data suggest that while *Dnmt3a* loss results in disease-specific DMRs, it also allows the persistence of HSPC-like methylation profiles in the leukemic blasts despite these cells expressing phenotypic differentiation markers that suggest maturity beyond HSPC.

Human AML is known to exhibit altered DNA methylation relative to normal HSPC (38, 39). As expected, we find that human *FLT3*-ITD AML exhibits extensive global DNA methylation changes compared to normal human HSC, irrespective of *DNMT3A* status (Supplementary Fig. 2A–B). However, comparison of *FLT3*-ITD *DNMT3A*-wild-type

versus *FLT3*-ITD *DNMT3A*-mutant AML reveals a more restricted pattern of predominantly hypomethylated DNA associated with *DNMT3A* mutation (Supplementary Fig. S2C). Similarly, comparison of murine MPN or AML versus wild-type LSK marrow cells reveals dramatic differences in global DNA methylation patterns (Supplementary Fig. S2D–E); however, comparing murine MPN versus murine AML reveals a more subtle global consequence of *Dnmt3a* haploinsufficiency, predominantly resulting in DNA hypomethylation (Supplementary Fig. S2F).

To understand whether these changes in global DNA methylation correspond to changes in gene expression, we performed RNA sequencing on c-Kit$^+$ splenocytes from murine AML and MPN (Fig. 2G, Supplementary Table S4). Similar to our findings in the methylome, the expression of some genes in murine AML blasts is similar to LSK marrow cells ("HSPC-like" Fig. 2G, Supplementary Table S4), while a group of mostly upregulated genes are uniquely expressed in AML compared to LSK or MPN ("AML-unique" Fig. 2G, Supplementary Table S4). In agreement with prior studies indicating that Dnmt3a regulates HSPC function (21, 40), Gene set enrichment analyses (GSEA) demonstrated that genes upregulated in murine AML are enriched for HSPC gene expression as well as genes downregulated during myeloid development (Supplementary Fig. S3A, Supplementary Table S4) (41, 42). To evaluate the relevance of murine *Flt3$^{ITD/ITD}$;Dnmt3a$^{fl/fl}$ MxCre* AML gene expression in human AML, we identified genes that are significantly upregulated in murine AML versus MPN, then curated a gene-set of their human orthologs (Supplementary Table S4). When we compare gene expression data from human *FLT3*-ITD AML with either wild-type or mutant *DNMT3A*, GSEA demonstrates that gene expression in *DNMT3A*-mutant AML is significantly enriched for this gene set (Fig. 2H). We then performed correlation (Fig. 2I) and GSEA analyses (Fig. 2J, Supplementary Table S4) between murine AML DMRs and gene expression, finding that the majority of overexpressed genes (60%) overlap with sites of DNA hypomethylation events in the murine AML (Fig. 2I, upper left quadrant red dots). Finally, we validated candidate genes with *Flt3$^{ITD/ITD}$;Dnmt3a$^{fl/fl}$ MxCre* AML-unique (*Emilin2* and *Pim1*) and HSPC-like (*Gata3*) DMRs and associated gene upregulation (Fig. 2K). We conclude that deletion of a single *Dnmt3a* allele results in functional Dnmt3a haploinsufficiency, and in the context of *Flt3$^{ITD/ITD}$* recapitulates a pattern of methylation and gene expression seen in human AML with *FLT3*-ITD and *DNMT3A* mutations.

GSEA also revealed that murine AML-upregulated genes are enriched for c-Myc-target-gene sets (Supplementary Fig. S3B and Supplementary Table S4). Therefore, we genetically incorporated a knock-in allele that generates an eGFP-c-Myc fusion protein from the endogenous *c-Myc* locus (*c-Myc^{eGFP};Flt3$^{ITD/ITD}$;Dnmt3a$^{fl/fl}$ MxCre* AML vs. *c-Myc^{eGFP};Flt3$^{ITD/ITD}$;Dnmt3a$^{fl/fl}$* MPN) (43). We found significantly increased levels of c-Myc^{eGFP} expression in c-Kit$^+$ splenocytes from AML versus MPN mice (Supplementary Fig. S4A); however, only a subpopulation of c-Kit$^+$ splenocytes from either genotype expressed c-Myc^{eGFP}. In contrast, when AML splenocytes are grown in cytokine rich media *in vitro* the majority express c-Myc^{eGFP}, but treatment with a Flt3 inhibitor (Quizartinib/AC220) downregulated c-Myc^{eGFP} (Supplementary Fig. S4B). Flow cytometric analysis of phospho-Stat5, a downstream effector of *Flt3^{ITD}* (28), was uniformly activated in c-Kit$^+$ AML splenocytes (Supplementary Fig. S4C). These data suggest that c-Myc^{eGFP} is a potential biomarker of *Flt3^{ITD}* signaling, but that there is significant heterogeneity in AML

cellularity and/or integration of *Flt3*^{ITD} and loss of Dnmt3a signaling. To assess this possibility, we dissected the cellular architecture of the murine AML model using single-cell RNA-Sequencing (scRNA-Seq) coupled to complementary single-cell assays. Using the Iterative Clustering and Guide-gene Selection (ICGS) algorithm in AltAnalyze (44), unsupervised analysis of 96 individual c-Kit^{+} AML splenocyte libraries (generated from two independent mice) identified 7 distinct cell populations. Based on gene expression and ontology analysis in GO-Elite (45) the cell clusters were assigned identities similar to their normal counterparts (macrophage-dendritic precursors "MDP" (46), neutrophil precursors, monocyte progenitors, and four distinct HSPC-like populations) (Fig. 3A, Supplementary Table S5). We note that more mature cell types express *c-Myc* with low incidence and amplitude (e.g. MDP and neutrophil precursors), while the more immature populations show high *c-Myc* incidence and amplitude (Fig. 3B). However, the bioinformatics assignment of a mature cellular identity does not necessarily obviate the leukemogenic potential of an AML subpopulation. Therefore, we performed flow cytometric sorting and CFU assays to assess the clonogenic potential of ICGS-defined murine AML subpopulations. Using discovered candidate markers from the ICGS clusters (*c-Kit, Cxcr4, c-Myc,* and *Il18r1)* (Fig. 3B), ten AML subpopulations were sorted using combinations of these markers (Fig. 3C; representative flow plots). While c-Kit^{+} AML cells contain the clonogenic fraction (Fig. 3D compare 1 vs. 3), c-Kit^{+}c-Myc^{eGFP} cells were significantly enriched for clonogenicity (Fig. 3D compare 2 and 3 vs. 4). Thus, although c-Kit^{+} splenocytes uniformly show activated Stat5 downstream of *Flt3*^{ITD} signaling, the heterogeneity in integrating that signal to provide c-Myc protein accumulation appears to be context dependent and most probably relates to the progenitor versus precursor-like state of the *Flt3*$^{ITD/ITD}$*;Dnmt3a*$^{fl/fl}$ *MxCre* AML cell.

We find, in contrast to c-Myc, Cxcr4^{+} expressing AML cells had reduced clonogenicity in all populations as compared to populations without surface Cxcr4 expression (Fig. 3D compare 3 vs. 6, 4 vs. 9, 5 vs. 7, and 8 vs. 10). Notably, while both *c-Myc* and *Cxcr4* are expressed at high amplitude and incidence in several ICGS clusters, only *c-Myc* is expressed at high incidence in the HSPC-like-1 cluster (Fig. 3B). Searching for another HSPC-like-1-enriched marker with amenable reagents for flow cytometry, we focused upon Interleukin 18 receptor 1 (*Il18r1,* Il18rα, or CD218a) (Fig. 3B). While Il18rα is expressed at very high levels in *Flt3*$^{ITD/ITD}$*;Dnmt3a*$^{fl/fl}$ *MxCre* AML, role for Il18rα in normal HSPC or AML has yet to be clearly defined (47). Similar to c-Kit^{+}c-Myc^{eGFP} cells, c-Kit^{+}Il18rα^{+} cells were enriched for clonogenicity (Fig. 3D population 3 vs. 5); however, AML cells that were triple-positive (c-Kit^{+}c-Myc^{GFP}Il18rα^{+}Cxcr4^{-}) were the most significantly enriched for leukemia clonogenicity (Fig. 3D population 8). In summary, the *Flt3*$^{ITD/ITD}$*;Dnmt3a*$^{fl/fl}$ *MxCre* AML model consists of functionally heterogeneous c-Kit^{+} stem/progenitor/precursor populations with enriched clonogenicity corresponding to HSPC-like cluster gene expression.

Given the association between DMR and gene expression (Fig. 2), and the considerable cellular heterogeneity in gene expression (Fig. 3), we next determined whether manipulating Dnmt3a levels would reverse methylation, gene expression and/or clonogenicity. To this end, we rescued *Dnmt3a* haploinsufficiency in the murine AML by forced expression of *DNMT3A* (Fig. 4A). Compared to empty vector (EV) control transduced AML, DNMT3A rescue did not alter differentiation or colony numbers in the initial plating (Fig. 4B, left bar

graphs). Importantly, DNMT3A rescue ablated clonogenicity upon replating (Fig. 4B, right line graphs), and was associated with DNA hypermethylation (Fig. 4C, Supplementary Table S6). In particular, 74/260 of the differentially methylated regions in AML were reverted to methylation levels similar to MPN and 40 new hypermethylated regions were identified (Fig. 4D). As in the *de novo* murine AML cells, there was a significant enrichment of DMRs overlapping with both intra- and intergenic enhancers (12% of DMRs at intragenic enhancers versus 3% background, $p<2.2x10^{-16}$ and 8% of DMRs at intergenic enhancers versus 2% background, $p<2.2x10^{-16}$) (Fig. 4E). In agreement with the association between HSPC-like gene expression and clonogenicity, prior to rescue the HSPC-like AML populations expressed genes proximal to re-methylated regions at a significantly higher level compared to more mature precursors (Fig. 4F, Supplementary Fig. S4D compare clusters c3–c7 versus c1 and c2). For example, we consistently observed DNA hypomethylation of the *Gata3*, *Cxxc5*, and *Hdac7* gene loci in both human and murine *Dnmt3a*-mutant AML (Supplementary Table S3). In addition, *GATA3* and *CXXC5* were overexpressed in human *FLT3*-ITD/*DNMT3A*-mut AML (Supplementary Table S4 GSEA leading edge from Fig. 2H), while *Gata3*, *Cxxc5*, and *Hdac7* were all significantly overexpressed murine AML (Fig. 2I, Supplementary Table S4). Moreover, *Gata3*, *Cxxc5*, and *Hdac7* were expressed almost exclusively in the HSPC-like murine AML subpopulations (Fig. 3B, Supplementary Fig. S4E) and are hypermethylated upon *DNMT3A* rescue (Fig. 4D). These data suggest that genes that respond in this manner may have central roles in CN-AML downstream of DNMT3A and FLT3. We conclude that DNA hypomethylation downstream of Dnmt3a loss-of-function is reversible.

Since DNMT3A rescue diminished the colony forming ability of $Flt3^{ITD/ITD};Dnmt3a^{fl/fl}$ *MxCre* AML we next sought to delineate genes downstream of Dnmt3a loss-of-function that might be important for leukemic potential. To this end, we examined the clonogenicity of murine c-Kit^{+} AML cells upon shRNA-mediated knockdown of genes that are overexpressed and hypomethylated in murine AML, and/or DMR reverted upon DNMT3A rescue (e.g. *Gata3*, *Emilin2*, *Hdac7*, *Cxxc5*, *Alpk3*, and *Ttyh2*). We also examined knockdown of *Il18r1* (Il18rα) on colony formation since we find this cell surface receptor is expressed on HSPC-like populations with increased clonogenicity (Fig. 3D). Repression of *Emilin2* and *Cxxc5* by multiple independent hairpins caused significant reduction in colony formation, while *Il18r1* knockdown had no effect (Fig. 4G and Supplementary Fig. S4F). Even though we did observe some reduction in colony formation with *Gata3* and *Alpk3* shRNA, these effects were less consistent across multiple hairpins in multiple mouse AMLs (data not shown); however, we cannot discount the possibility that these genes may also play a role in $Flt3^{ITD/ITD};Dnmt3a^{fl/fl}$ *MxCre* AML. In sum, these data suggest Il18rα simply serves as a surface marker on AML cells with increased clonogenic capacity, while *Cxxc5* and *Emilin2*, which are specifically expressed in HSPC-like AML populations, have an important functional role in self-renewal and proliferation *in vitro*. In conclusion, Dnmt3a haploinsufficiency collaborates with $Flt3^{ITD}$ to form a rapidly lethal, fully penetrant, AML. Dnmt3a loss is associated with reversible changes in DNA methylation leading to signaling programs distinct from $Flt3^{ITD}$ alone that promote leukemogenesis.

Discussion

Flt3^{ITD} mutation combined with other oncogenic lesions such as *Tet2*$^{-/-}$ (16), *Mll*^{PTD} (35), and Npmc^{+} (48) progress to AML or mixed lineage leukemias in mice. The uniquely rapid lethal nature of the *Flt3*$^{ITD/ITD}$*;Dnmt3a*$^{fl/fl}$ *MxCre* AML model may be due to Dnmt3a control of HSC self-renewal. Deletion of *Dnmt3a* (*Dnmt3a*$^{-/-}$) specifically expands HSC and myeloproliferation *in vivo*, but does not produce acute leukemia (21, 49). The addition of *KRas*^{G12D} mutation with *Dnmt3a*$^{-/-}$ in mice significantly accelerates MDS/MPN development compared to *KRas*^{G12D} alone (50). Yet only ~30% of *Dnmt3a*$^{-/-}$*;KRas*^{G12D} *MxCre* mice progress to AML and require pIpC to induce complete *Dnmt3a* deletion. The *DNMT3A-R882H* mutation found in human AML acts as a dominant negative that reduces, but does not completely block, the activity of DNMT3A (18). Moreover, the prognosis for human *FLT3*-ITD AML is worsened with the addition of a *DNMT3A* mutation (3, 12, 13). In parallel to human *FLT3*-ITD/*DNMT3A*-mutant CN-AML, *Flt3*$^{ITD/ITD}$*;Dnmt3a*$^{fl/fl}$ *MxCre* mice spontaneously select for *Dnmt3a* haploinsufficiency –rather than a complete loss– that transforms *Flt3*^{ITD} MPN into a rapidly lethal AML with 100% penetrance. Moreover, a high *FLT3*-ITD allelic ratio predicts poor survival in human AML (51). Thus, the requirement for two *Flt3*^{ITD} alleles to form AML (in cooperation with Dnmt3a loss) in this mouse model is consistent with human disease. The pattern of methylation was similar to human AML with *FLT3*-ITD and mutations in *DNMT3A*. In addition, there was significant correlation between the expression of some genes with nearby changes in DNA methylation in *Flt3*$^{ITD/ITD}$*;Dnmt3a*$^{fl/fl}$ *MxCre* AML compared to *Flt3*$^{ITD/ITD}$*;Dnmt3a*$^{fl/fl}$ MPN, indicating that these changes in DNA methylation do not reflect non-specific methylation losses but rather play a functional role in the development of leukemia.

We used single cell RNA-Seq to dissect the cellular architecture of the leukemia. While cancer stem cell markers are usually not conserved across different cancers (46), c-Kit expression is a known marker of leukemia stem cells (LSC) in other AML models. In agreement with this, our functional assays revealed tremendous enrichment for clonogenicity in the c-Kit^{+} population. However, the scRNA-Seq analysis revealed significant heterogeneity within the c-Kit^{+} leukemic splenocytes, with many subpopulations expressing transcriptomes similar to myeloid precursors and possessing little clonogenicity. In contrast, expression of Il18rα (CD218a) significantly enriched clonogenic potential in our murine AML model. Manipulation of *Il18r1* (Il18rα) by shRNA in *Flt3*$^{ITD/ITD}$*;Dnmt3a*$^{fl/fl}$ *MxCre* AML cells had no significant effect on colony forming ability. Therefore, Il18rα is a candidate surface marker of a rare leukemia stem cell population, but is likely not driving the functional clonogenic output. In addition to Il18rα and c-Kit, the most highly clonogenic subpopulation also accumulated c-Myc protein and expressed significantly higher levels of HSPC-like genes, whose associated DMR were reverted upon DNMT3A rescue. Therefore, this rare putative LSC population contained active oncogenic signaling downstream of mutant Dnmt3a and Flt3^{ITD}, demonstrating the power of single cell analyses to resolve both biological and molecular complexity.

The correlation between reverted DMR and significantly diminished clonogenicity in our murine AML suggests that the methylome changes downstream of mutant DNMT3A in human AML are probably disease-driving and reversible. *Cxxc5* is an exemplary candidate

because it conforms to many criteria of a functionally important putative Dnmt3a target gene in AML; hypomethylated and overexpressed (HSPC-like) in murine and human AML, DMR reverted upon DNMT3A rescue, and knockdown of *Cxxc5* (similar to DNMT3A rescue) significantly diminished AML colony forming ability. The CXXC-type zinc finger protein Cxxc5 is a pleiotropic factor that can interact with Dishevelled to inhibit Wnt/β-catenin signaling (52, 53), binds to CpG-rich DNA sequences to regulate gene expression (54), and is a biomarker and potential therapeutic target in leukemia (55–57). The extracellular matrix protein Emilin2, also described as an inhibitor of Wnt signaling (58), is hypomethylated and overexpressed in AML, and is important for AML clonogenicity. Since both Cxxc5 and Emilin2 play a role in Wnt signaling and c-Myc is a target of the Wnt pathway, we monitored the level c-Myc^{GFP} and do not find that shRNA-knockdown of either *Cxxc5* or *Emilin2* disrupt c-Myc accumulation (data not shown). Though this does not preclude a possible role for either Cxxc5 or Emilin2 in Wnt signaling, more work needs to be done to fully understand the roles and therapeutic potential of Cxxc5 and Emilin2 in *FLT3*-ITD *DNMT3A* mutant AML.

Our data suggest that the functional implications of some cancer-specific epigenetic alternations (e.g. DNMT3A mutations) may extend beyond that of persisting clones from the pre-malignant state (59, 60) to a continuing role in AML disease pathogenesis and maintenance. We note recent progress in small molecule inhibitors therapeutically targeting proteins that create and/or maintain epigenetic modifications in cancer. Given the acutely rapid and spontaneous development of AML in the *Flt3*$^{ITD/ITD}$*;Dnmt3a*$^{fl/fl}$ *MxCre* mice, and the plasticity of DNA methylation within the resulting AML, we conclude that this new murine model is suitable for testing future therapeutic methods of manipulating Dnmt3a, which may provide new opportunities for clinical intervention in CN-AML.

Methods

Animals

Mice were bred and housed by Cincinnati Children's Hospital Medical Center (CCHMC) Veterinary Services, and mouse manipulations were performed according to protocol reviewed and approved by the Children's Hospital Research Foundation Institutional Animal Care and Use Committee (Protocol Number IACUC 2013-0090). *c-Myc*^{eGFP} (43), *Flt3*^{ITD} (27), *Dnmt3a*^{flox} (61), *Mx1Cre* (62), mice were maintained on the C57BL/6-Ly5.2 (CD45.2) background. CD45.1^{+} C57BL/6-Ly5.1 (JAX and CCHMC Comprehensive Mouse Core) transplant recipient mice were between 1–3 months of age and given 700 Rads 5 hours prior to tail vein injection of single cell suspensions.

Bone Marrow and Leukemic Splenocyte Isolation

Moribund mice were euthanized with carbon dioxide and cervical dislocation. Cytospin Buffer containing 10% FBS (HyClone), 2% BSA Fraction V (ThermoFisher Scientific), and Cell Dissociation Buffer (Gibco) in PBS was used for all cell isolations, washes, and cytospins under sterile conditions. Bone marrow cells were isolated from freshly sacrificed mice by crushing bones using a mortar and pestle. Splenocytes were isolated from freshly sacrificed mice and crushed between two glass slides. Red blood cells were lysed using

Ammonium-Chloride-Potassium (ACK) buffer (Gibco), washed, and filtered to obtain single cells suspensions for downstream applications.

Histology and cytospins

Bone marrow, spleen, liver, and sternum here harvested from moribund *Flt3*$^{ITD/ITD}$*;Dnmt3a*$^{fl/fl}$ *MxCre* and age-matched wild-type or *Flt3*$^{ITD/ITD}$*;Dnmt3a*$^{fl/fl}$ controls. Sternum was decalcified then spleen, liver, and sternum were paraffin embedded and sections were stained with hematoxylin & eosin (H&E) (CCHMC pathology core) and cytospins were stained with Wright Giemsa using the Camco Stain Pak (Cambridge Diagnostic Products). Cytospins of bone marrow and spleen were performed both before and after red blood cell lysis. Photographs were taken on a Nikon Eclipse 80i microscope with a Nikon Digital Sight camera using NIS-Elements F4.30 software at a resolution of 2560 × 1920. Using Adobe Photoshop CS2, auto contrast was applied to H&E images, unsharp mask was used to improve image clarity, images were re-sized and set at a resolution of 300 pixels/inch, and variations was used to adjust color balance and brightness. Scale bar represents 30μm in each image. At least 3–5 mice per group were examined for histologic, morphologic, peripheral blood, and flow cytometric findings for acute myelomonocytic leukemia diagnosis.

Spectral Karyotyping Analyses

To characterize the cytogenetic pattern of AMLs from *Flt3*$^{ITD/ITD}$*;Dnmt3a*$^{fl/fl}$ *MxCre* mice, G-banding and SKY analysis was performed using the ASI SkyPaint™ assay for mouse chromosomes as described previously (63) on fresh or viably frozen bone marrow and spleen cells moribund mice with leukemia. Five independently derived AMLs (20 metaphases per case) from the *Flt3*$^{ITD/ITD}$*;Dnmt3a*$^{fl/fl}$ *MxCre* model were analyzed. The analysis of 20 cells excludes an abnormal clone of ≥14% with 95% confidence.

Flow cytometry and cell sorting

All flow cytometric staining, sorting, and analyses were performed by resuspending cells in 1X FACS Buffer (1% FBS, 0.01% NaN_3 in DPBS). To isolated c-Kit$^+$ leukemic stem/progenitor populations, freshly isolated single cells suspensions were incubated with CD117 MicroBeads and separated on an AutoMACS Pro separator (Miltenyi, San Diego, CA) according to manufacturer specifications.

To prepare for flow cytometric analysis of stem/progenitor populations, single cell suspensions were first stained with a cocktail of biotin-conjugated antibodies against markers of lineage positive cell types: anti-CD3 (clone 145-2C11, BioLegend, San Diego, CA), anti-CD4 (clone RM4-5, eBioscience, San Diego, CA), anti-CD8 (clone 53-6.7, Becton, Dickinson and Company, Franklin Lakes, NJ), anti-CD11b (clone M1/70, Becton, Dickinson and Company), anti-CD19 (clone 6D5, BioLegend), anti-Gr1 (clone RB6-8C5, BioLegend), anti-Ter119 (clone Ter-119, BioLegend) and anti-CD45R (clone RA3-6B2, BioLegend). Following two washes in 1X FACS Buffer, lineage stained cells were stained with: Streptavidin-conjugated APC-Cy7 (Becton, Dickinson and Company), PerCP-eFluor710-conjugated anti-CD16/32 (clone 93, eBioscience), APC-conjugated anti-CD117 (clone 2B8, Becton, Dickinson and Company), PE-Cy7-conjugated anti-Sca1 (clone D7,

Becton, Dickinson and Company) and BV421-conjugated anti-CD34 (clone RAM34, Becton, Dickinson and Company). Alternatively, for analysis of L-GMP populations, a modified lineage cocktail was used, which excluded anti-CD11b and anti-Gr1 biotin-conjugated antibodies. Furthermore, lineage stained cells were incubated with the same antibodies described above but with BV605-conjugated anti-CD11b (clone M1/70, Becton, Dickinson and Company) and PE-Cy5-conjugated anti-Gr1 (clone RB6-8C5, eBioscience) added and BV650-conjugated anti-CD117 (clone RAM34, Becton, Dickinson and Company) substituted for the APC-conjugate. Antibodies were used at 1:100 dilutions, except for anti-CD34, which was used at 1:50 in a staining volume of 50μl/5x10^6 cells. All results reported for LK, GMP, and LSK populations exclude CD11b and Gr1 along with other linage markers indicated above either as biotin or fluorochrome conjugates.

To prepare for flow cytometric analysis of mature populations, single cell suspensions were incubated with FcγRII/III Block (clone 2.4G2, Becton, Dickinson and Company) and a combination of: Pacific Blue-conjugated anti-CD11b (cloneM1/70, BioLegend), PE-Cy7-conjugated anti-Gr1 (clone RB6-8C5, BioLegend), APC-conjugated anti-CD3 (clone 145-2C11, Becton, Dickinson and Company) or FITC-conjugated anti-CD3 (clone 145-2C11, Becton, Dickinson and Company), PE-conjugated anti-CD45R (clone RA3-6B2) or AlexaFluor700-conjugated anti-CD45R (clone RA3-6B2, BioLegend), PerCP-Cy5.5-conjugated anti-CXCR4 (clone L276F12, BioLegend) PE-conjugated anti-IL18R (clone P3TUNYA, eBioscience), and APC-conjugated anti-CD117 (clone RAM34, Becton, Dickinson and Company) or BV650-conjugated anti-CD117 (clone RAM34, Becton, Dickinson and Company). Antibodies were used at 1:100 dilutions in a staining volume of 50 μl for up to 5x10^6 cells.

Cell sorting was performed on a MoFloXDP (Beckman Coulter, Brea, CA) or BD FACSAria II with a 70μm or 100μm nozzle. Sorted populations of interest were collected in DPBS buffer containing 50% FBS (Hyclone). Flow cytometric analyses were performed on a FACS LSRII or LSR Fortessa (Becton, Dickinson and Company). Data were analyzed with FlowJo Software (TreeStar, Ashland, OR).

In preparation for flow cytometric analysis of phospho-STAT5 quantitation, one million freshly isolated c-Kit^+ splenocytes were added to each well of a 96-well round bottom plate and centrifuged at 300xg at 4°C for 5 minutes. Cells were next fixed in 100μl of 4% methanol-free formaldehyde (Pierce) for 20 minutes at room temperature and then centrifuged as before. Cells were washed in 200 μl 1X FACS Buffer. Next, cells were permeabilized for 10 minutes at 4°C in 200μl of 90% methanol (Fisher) then washed twice. Cells were stained with PE-conjugated anti-phosphoY694-Stat5 antibody (clone 47/Stat5-pY694, Becton, Dickinson and Company) at a 1:100 dilution in 100μl of 1X FACS buffer for 1 hour on ice. Cells were washed twice prior to flow analysis.

AC220 treatment

Prior to *in vitro* treatment with AC220 (Ambit Biosciences), cryopreserved splenocytes were thawed and cultured overnight in StemSpan (Stem Cell Tech) supplemented with recombinant mouse IL3 (10 ng/ml), IL6 (20 ng/ml), and SCF (25 ng/ml) (Miltenyi). Cells were then replated at 1 million cells per ml with either 0.1% DMSO or 1nM AC220 and

incubated for 5 hours at 37°C. Cells were then washed once in 1X FACS and stained with APC-conjugated anti-CD117 (clone RAM34, Becton, Dickinson and Company) at a 1:100 dilution in 100μl of 1X FACS buffer for 1 hour on ice. Cells were washed twice prior to flow analysis.

RNA Isolation, cDNA synthesis, and TaqMan Assay

RNA was extracted using TriZol or TriZol LS (Ambion) as previously described (64). Total RNA was converted into cDNA using the High Capacity cDNA Archive Kit (Life Technologies) for standard gene expression analyses. All gene expressions were quantified using TaqMan assays (Life Technologies) with the 2x Universal TaqMan Master Mix (Life Technologies) according to the manufacturers instructions on the StepOne *Plus* Instrument (Applied Biosystems, Inc.) using equal amounts of starting cDNA. Standard inventoried gene expression TaqMan assays recommended by the manufacturer (Life Technologies) for best coverage were purchased when available. For human gene expression assays: *DNMT3A* (Hs01027166_m1). For mouse gene expression assays: *Dnmt3a* (Mm00432881_m1), *Emilin2* (Mm00467425_m1), *Pim1* (Mm00435712_m1), *Gata3* (Mm00484683_m1), *Cxxc5* (Mm00505000_m1), *Il18r1* (Mm00515178_m1). Gene expression data was analyzed using the comparative Ct method ($2^{-\Delta\Delta Ct}$). Human *SDHA* (Hs00417200_m1) and mouse *Sdha* (Mm01352366_m1) served as loading controls.

Bulk RNA Sequencing Analyses

c-Kit$^+$ splenocytes were harvested from three independent *Flt3*$^{ITD/ITD}$*;Dnmt3a*$^{fl/fl}$ *MxCre* or age-matched *Flt3*$^{ITD/ITD}$*;Dnmt3a*$^{fl/fl}$ mice. RBCs were lysed with ACK, and 5x10^6 leukemia cells were lysed with TriZol (Invitrogen). RNA quality and quantity were measured by Agilant Bioanalyzer at CCHMC Microarray Core. Then samples with a RIN>8.0 were processed by poly-A selection, stranded True-seq protocol and RNA library sequencing using paired-end 75bp reads at a depth of 40 million paired-reads per sample (Illumina HiSeq 2500) by the CCHMC Sequencing Core. Sorted LSK, CMP and GMP bulk RNA sequenced samples, obtained using the same library preparation and sequencing protocol were obtained from the gene expression omnibus dataset GSE70235. The fastq files were aligned to mouse genome Mm10 using BowTie2 and TopHat 2 (65, 66). Gene level RPKM (Reads Per Kilobase of transcript per Million mapped reads) were obtained using AltAnalyze 2.0.9 (44) to identify differentially expressed genes between *Flt3*$^{ITD/ITD}$*;Dnmt3a*$^{fl/fl}$ *MxCre* AML and *Flt3*$^{ITD/ITD}$*;Dnmt3a*$^{fl/fl}$ MPN using default parameters, including a moderated t-test with Benjamini-Hochberg multiple testing correction, raw p-value cut-off of 0.05, RPKM>1 and a differential expression cut-off of 2-fold. WT LSK samples were also displayed as normal baseline comparators. HOPACH (Hierarchical Ordered Partitioning And Collapsing Hybrid) clustering in AltAnalyze was used to identify clusters of gene expression in AML, MPN, and WT LSK.

Single Cell RNA Sequencing Analyses

Single CD117$^+$ (c-Kit$^+$) cells were prepared using the C1™ Single-Cell Auto Prep System (Fluidigm, San Francisco, CA), according to the manufacturer's instructions. In short, sorted cells were counted and resuspended at a concentration of 333,333 cells per 1 ml DPBS then loaded onto a primed C1 Single-Cell Auto Prep Integrated Fluidic Chip for mRNA-Seq (5–

10 μm). After the fluidic step, cell separation was visually scored to identify wells containing single live cells. In two independent rounds, 52 and 56 cells were captured. Cells were lysed on the chip and reverse transcription was performed using the Clontech SMARTer® Kit with the mRNA Seq: RT + Amp (1771x) according to the manual. After the reverse transcriptase step, cDNAs were transferred to a 96-well plate and diluted with 6μl C1™ DNA Dilution Reagent. cDNAs were quantified using the Quant-iT™ PicoGreen® dsDNA Assay Kit (Life Technologies, Grand Island, NY) and Agilent High Sensitivity DNA Kit (Agilent Technologies (Santa Clara, CA). Libraries for the first 48 visually validated cells from each of the two independent captures were prepared using the Nextera XT DNA Library Preparation Kit (Illumina Inc., Santa Clara, CA). In each single-cell library preparation, a total of 125pg cDNA was tagmented at 55°C for 20 minutes. Next, libraries were pooled and purified on the AMPure® bead-based magnetic separation Kit prior to a final quality control check using both the Qubit® dsDNA HS Assay Kit (Life Technologies, Grand Island, NY) and Agilent High Sensitivity DNA Kit. The majority of cDNA fragments were confirmed to be between 200–602 base pairs (bp), qualifying the libraries for sequencing. All 96 single-cell RNA-Seq libraries were sequenced on one HiSeq 2500 gel. Gene expression was quantified as transcripts per million (TPM) using RSEM (RNA-Seq by Expectation-Maximization) alignment and quantification (67). The predominant gene expression signatures were obtained from the ICGS (Iterative Clustering and Guide-gene Selection) module of AltAnalyze 2.0.9 (http://altanalyze.org/ICGS.html). For ICGS analysis, genes with a minimum TPM>1 and fold>4 in at least 3 cells were retained for analysis, with a minimum Pearson correlation cutoff of 0.4 and conservative exclusion of cell-cycle effects selected as the parameters. Associated cell population predictions were obtained the GO-Elite (45) module in AltAnalyze and verified based on prior literature. All associated expression plots display gene expression values as the median subtracted or un-subtracted $\log_2$ TPM values. The genes associated with DNMT3A rescued AML reverted DMRs are displayed in Violin plots comparing the expression of these genes in the original single cell RNA-Seq AML dataset across all clusters using the vioplot library in R.

Human AML specimens

Genomic DNA was isolated from bone marrow mononuclear cells from AML leukemia patients seen either at Erasmus Medical Center, Rotterdam or enrolled in the E1900 clinical trial from the Eastern Cooperative Oncology Group. Informed consent was obtained prior to sample banking. IRB approval for this study was obtained at the University of Michigan and Weill Cornell Medical Center. This study was performed in accordance to the declaration of Helsinki. All specimens analyzed age-matched consisted of >90% blasts. A total of 32 patients were included (Supplementary Table S7). Sixteen patients were *FLT3*-ITD/*DNMT3A*-wt while 13 patients were *FLT3*- ITD/*DNMT3A*-mut. All patients were wild-type for *TET2, IDH1* and *IDH2*. Patients with *FLT3*-TKD were also excluded. Bone marrow from normal donors was obtained after IRB approval from the Johns Hopkins Sidney Kimmel Cancer Center Specimen Accessioning Core. Mononuclear cells were isolated by density centrifugation using Ficoll-Paque PLUS (GE Healthcare) and then labeled for CD34 positive selection using the CD34 MicroBead kit (Miltenyi Biotec) and frozen viable in FBS + 10% DMSO. Upon thawing, CD34+ cells were labeled using the Aldefluor kit (Stem Cell Technologies), CD34-BV421 or CD34-PE-Cy7, CD45-PE, CD38-APC (BD Biosciences)

and 7-Aminoactinomycin D (7-AAD; Life Technologies). Hematopoietic stem cells (HSC) were identified as $ALDH^{high}CD34^{+}CD38^{-}CD45^{+}$, and sorted on a Beckman Coulter MoFlo in the Cell Sorting Core Facility at the Johns Hopkins Bloomberg School of Public Health. Gene expression data for these AML patients was previously published (68) (GEO accession number: GSE6891).

DNA Isolation and Dnmt3a Genotyping

DNA was isolated from c-Kit^{+} splenocytes (ERRBS) or single cell suspensions from individual colonies grown for 7 days in methylcellulose (genotyping) using the Qiagen Puregene kit according to manufacturer's instructions. For small cell numbers glycogen was added to help precipitate DNA. ERRBS data for wild-type murine LSK cells were previously published (69) (GEO accession number: GSE57114). For genotyping the Dnmt3afl/fl-F 5′-TGT GGC ATC TCA GGG TGA T -3′, Dnmt3afl/fl-R 5′-CTC AGG CCC TCT AGG CAA G -3′, and Dnmt3aKO-R 5′-GAA GCA GCA GTC CCA GGT AG -3′ were used.

DNA methylation by ERRBS

Enhanced Reduced Representation Bisulfite Sequencing (ERRBS) libraries were generated from 25ng of genomic DNA as previously described (37) for the human specimens, and sequenced on a HiSeq-2000 sequencer. Murine libraries were prepared in the same way but using the indexed adaptors and sequenced with two libraries per lane on a HiSeq-2500 sequencer (70). Reads were aligned against a bisulfite-converted version of the hg19 or mm9 builds of the genome using Bowtie followed by methylation percentage calling using Bismark (71). Conversion rates were >99.8 for all samples. Only genomic regions with coverage between 10X and 500X were included for downstream data analysis.

DNA methylation data analysis

ERRBS data analysis was performed using R statistical software version 3.0.3 and the MethylSig 0.1.3 package (72) for differential methylation calling using the beta binomial method. The MethylKit 0.9.2.5 package (73) was used for downstream gene-, CpG-, and enhancer region annotation analysis and, chromosome ideogram representations. Differentially methylated regions (DMR) were identified by first summarizing the methylation status of genomic regions into 25-bp tiles and then identifying regions with absolute methylation difference ≥25% and false discovery rate (FDR) <10%. DMRs were annotated to GENCODE genes using a custom script with the following criteria: (i) DMRs overlapping with a gene were annotated to that gene, (ii) intergenic DMRs were annotated to all neighboring genes within a 50-kb window, and (iii) if no gene was detected within a 50-kb window, then the DMR was annotated to the nearest transcription start site (TSS) (74). Statistical significance for comparisons between all measured CpGs (all tiles) and DMRs at genomic, CpG, and enhancers regions was calculated using upper and lower tail binomial tests, percent of total DMR and p-values are reported.

Virus Production and Transduction

For virus production, Lenti-X 293T cells (Clonetech) were seeded at $4x10^6$ cells/10cm dish in standard growth medium DMEM (ThermoFisher Scientific) with 10% heat-inactivated FBS (Atlanta Biologics), Penicillin-Streptomycin (Pen-Strep) (ThermoFisher Scientific), and L-Glutamine (ThermoFisher Scientific). The following day, cells were replenished with fresh Opti-MEM GlutaMAX media (ThermoFisher Scientific) supplemented with 10% heat-inactivated FBS (Atlanta Biologics) at least two hours prior to transfection. MSCV-DNMT3A-GFP and empty vector MSCV-GFP retroviral plasmids were a kind gift from Dr. Grant Challen (Washington University, St. Louis). For retroviruses, 10μg of DNMT3A and empty vector (EV) retroviral vectors were co-transfected with 10μg retroviral packaging and envelope plasmid pCL-Eco (75) into Lenti-X 293T cells using Transit-LT1 (Mirus) according to manufacturer instructions. Virus-containing supernatant was collected 48 and 72 hours post-transfection, and either used immediately or frozen at −80°C in aliquots. For lentiviruses, gene targeting shRNA or non-targeting control lentiviral vectors were co-transfected with lentiviral packaging plasmid Δ8.9 (76) and envelope plasmid VsVg (77) using TransIT-LT1 (Mirus Bio) into Lenti-X 293T cells (Clonetech). Virus-containing supernatant was collected 48 and 72 hours post-transfection, and either used immediately or frozen at −80°C in aliquots. Two independent shRNA against *Cxxc5* (TRCN0000143369, TRCN0000219528), *Emilin2* (TRCN0000257587, TRCN0000246910), *Il18r1* (TRCN0000068103, TRCN0000068105) were purchased from the CCHMC Lenti shRNA viral Core or Sigma.

Transduction of c-Kit^+ leukemic splenocytes with retroviruses was performed using the spinfection method. Tissue culture plates were pre-coated with $5μg/cm^2$ recombinant Retronectin (Takara) overnight at 4°C, then blocked with 2% BSA (ThermoFisher Scientific) in PBS (ThermoFisher Scientific) for 30 minutes at RT. Unconcentrated fresh or freeze/thawed retroviral supernatant was spun onto the retronectin at 1,000g for 2 hours at 4°C. Supernatant was removed and a second spin was performed with additional retrovirus supernatant. Viral supernatant was removed and $1x10^6$ c-Kit^+ AML cells in 0.5ml standard growth medium were spun onto the retrovirus/retronectin coated wells at 1,000g for 10 minutes at RT. Then plates were removed overnight to 37°C 5% CO_2. The spinfection protocol was repeated again the next day. 48 hours post-transduction cells were sorted for GFP^+ expression, and 2,000 cells were plated in methylcellulose M3434 supplemented in triplicate. After 7 days colonies were enumerated, single cell suspensions were made, and 2,000 cells were serially replated in triplicate. Extra cells not replated were mixed with cell lysis solution (Qiagen) (for DNA isolation) or lysed in TriZol (for RNA isolation).

For lentiviral transduction, c-Kit^+ leukemic splenocytes freshly harvested from moribund AML mice were cultured overnight in standard growth medium RPMI 1640 (Thermo Fisher Scientific) containing 20% FBS (HyClone) supplemented with mouse recombinant SCF (60ng/ml), IL6 (20ng/ml), and IL3 (20ng/ml) (Miltenyi Biotech). $1x10^6$ c-Kit^+ leukemia cells in 400μl standard growth medium containing FBS were mixed with 100μl lentiviral supernatant. Cytokines (60ng/ml SCF, 20ng/ml IL6 and IL3) and polybrene (10μg/ml, Sigma) were added to the final volume. Cells were incubated with virus for 6 hours at 37°C with 5% CO_2, then virus supernatant was replaced with standard growth medium containing

FBS and cytokines. Cells were incubated for 48 hours, then for an additional 48 hours with 1.5μg/ml puromycin in fresh growth medium. 4,000 puromycin-selected cells were plated in triplicate in methylcellulose M3434 (Stem Cell Technologies) for colony forming assay. Colonies were enumerated after 7 days. Extra cells (not plated for colony assays) were lysed in TriZol (for RNA isolation).

GSEA Analyses

Log_2 RNA-Seq expression derived from c-Kit$^+$ leukemic splenocytes from three independent *Flt3*$^{ITD/ITD}$*;Dnmt3a*$^{fl/fl}$ *MxCre* AML mice and three *Flt3*$^{ITD/ITD}$*;Dnmt3a*$^{fl/fl}$ MPN mice was imported into GSEA v.2.2.0 (41, 42). A fold-change ranked gene list was created comparing the AML vs. MPN using the Diff_of_Classes ranking metric and genes were sorted by descending order real mode. GSEA analyses were run using 1,000 gene_set permutations of gene sets in the website gene matrix database with the weighted enrichment statistic. Results are reported for the most highly positively correlated and negatively correlated hematopoietic-related gene sets with leading edge analyses.

Genes upregulated in *Flt3*$^{ITD/ITD}$*;Dnmt3a*$^{fl/fl}$ *MxCre* AML versus murine MPN were tested for enrichment in human *FLT3*-ITD/*DNMT3A*-mut AML in GSEA as described above using a pre-ranked fold change gene expression list in descending order comparing *FLT3*-ITD/*DNMT3A*-mut AML versus *FLT3*-ITD/*DNMT3A*-wt AML. Genes upregulated in *Flt3*$^{ITD/ITD}$*;Dnmt3a*$^{fl/fl}$ *MxCre* AML both legacy and unique groups were used as the testing gene set. A gene set of nearest gene neighbors to hypo-methylated regions in *Flt3*$^{ITD/ITD}$*;Dnmt3a*$^{fl/fl}$ *MxCre* AML versus MPN was tested for enrichment in against a fold-changed ranked gene expression list from RNA-Seq. in *Flt3*$^{ITD/ITD}$*;Dnmt3a*$^{fl/fl}$ *MxCre* AML versus *Flt3*$^{ITD/ITD}$*;Dnmt3a*$^{fl/fl}$ MPN as described above.

In Vitro Colony Forming Assays

Equal numbers of cells were mixed with methylcellulose M3434 complete with cytokines SCF, IL6, IL3, and EPO (Stem Cell Technologies) according to manufacturers instructions in triplicate. 2,000 c-Kit$^+$ or c-Kit$^-$ cells where indicated were seeded per plate. On day 7 immortalized/transformed colonies >500 cells were enumerated. Colonies were dissociated with PBS, single cell suspensions were counted and either equal numbers of cells were replated, or used in other indicated downstream applications. Each group was performed in triplicate and results were repeated in independent experiments at least twice.

Statistical Analyses

The absolute cell numbers of mouse normal, MPN, and AML total bone marrow and spleen counts were converted to natural log prior to statistical evaluation to normalize the variance between groups. Significant differences between normal, MPN, and AML groups for each population were examined by two-way ANOVA with Tukey's multiple comparisons correction. The average cell counts are shown for at least 3 mice/group. The percentage of total bone marrow and spleen LK, GMP, and LSK and spleen CD11b$^+$Gr1$^+$CD3$^-$, CD11b$^+$Gr1$^-$CD3$^-$, and CD11b$^+$Gr1$^-$B220$^-$ populations are shown for at least 3 mice/group. Significant differences between normal, MPN, and AML groups for each population

were examined by two-way ANOVA with Tukey's multiple comparisons correction. Descriptions of statistical analyses used can also be found in the figure legends.

Supplementary Material

Refer to Web version on PubMed Central for supplementary material.

Acknowledgments

The authors would like to acknowledge the Cornell University Epigenetics Core, the University of Michigan Epigenomics Core facility, the Cincinnati Children's Hospital Pathology, Flow Cytometry, Gene Expression, and Comprehensive Mouse Cores. We also thank Dr. Peter Valk (Erasmus University Medical Center, Netherlands) for human AML samples and gene expression data. *c-Myc*^{eGFP} knock-in mice were a kind gift from Barry Sleckman (Washington University, St. Louis). *Dnmt3a*$^{fl/fl}$ mice were a kind gift from David Hildeman (CCHMC). DNMT3A retroviral constructs were a kind gift from Grant Challen (Washington University, St. Louis).

Grant Support

The research was supported by Ladies Auxiliary to the Veterans of Foreign Wars (LAVFW) Postdoctoral Fellowship (to S.E.M.), CancerFree KIDS (Loveland, Ohio), University of Cincinnati training grant NIEHS T32ES007250 (to S.E.M.), CCTST Just-InTime Core Grant Program (University of Cincinnati and CCHMC), Leukemia and Lymphoma Society Translational Research Program Award, NHLBI Progenitor Cell Biology Consortium U01HL099997 (to N.S.) and NIH R01CA159845 and R21CA186945 (to H.L.G.).

References

1. Dohner K, Dohner H. Molecular characterization of acute myeloid leukemia. Haematologica. 2008; 93(7):976–82.10.3324/haematol.13345 [PubMed: 18591623]
2. CGARN CGARN. Genomic and epigenomic landscapes of adult de novo acute myeloid leukemia. N Engl J Med. 2013; 368(22):2059–74.10.1056/NEJMoa1301689 [PubMed: 23634996]
3. Patel JP, Gonen M, Figueroa ME, Fernandez H, Sun Z, Racevskis J, et al. Prognostic relevance of integrated genetic profiling in acute myeloid leukemia. N Engl J Med. 2012; 366(12):1079–89.10.1056/NEJMoa1112304 [PubMed: 22417203]
4. Kiyoi H, Naoe T, Nakano Y, Yokota S, Minami S, Miyawaki S, et al. Prognostic implication of FLT3 and N-RAS gene mutations in acute myeloid leukemia. Blood. 1999; 93(9):3074–80. [PubMed: 10216104]
5. Schnittger S, Schoch C, Dugas M, Kern W, Staib P, Wuchter C, et al. Analysis of FLT3 length mutations in 1003 patients with acute myeloid leukemia: correlation to cytogenetics, FAB subtype, and prognosis in the AMLCG study and usefulness as a marker for the detection of minimal residual disease. Blood. 2002; 100(1):59–66. [PubMed: 12070009]
6. Thiede C, Steudel C, Mohr B, Schaich M, Schakel U, Platzbecker U, et al. Analysis of FLT3-activating mutations in 979 patients with acute myelogenous leukemia: association with FAB subtypes and identification of subgroups with poor prognosis. Blood. 2002; 99(12):4326–35. [PubMed: 12036858]
7. Kottaridis PD, Gale RE, Frew ME, Harrison G, Langabeer SE, Belton AA, et al. The presence of a FLT3 internal tandem duplication in patients with acute myeloid leukemia (AML) adds important prognostic information to cytogenetic risk group and response to the first cycle of chemotherapy: analysis of 854 patients from the United Kingdom Medical Research Council AML 10 and 12 trials. Blood. 2001; 98(6):1752–9. [PubMed: 11535508]
8. Tefferi A, Lim KH, Levine R. Mutation in TET2 in myeloid cancers. N Engl J Med. 2009; 361(11): 1117. author reply -8. 10.1056/NEJMc091348 [PubMed: 19741235]
9. Delhommeau F, Dupont S, Della Valle V, James C, Trannoy S, Masse A, et al. Mutation in TET2 in myeloid cancers. N Engl J Med. 2009; 360(22):2289–301.10.1056/NEJMoa0810069 [PubMed: 19474426]

10. Ley TJ, Ding L, Walter MJ, McLellan MD, Lamprecht T, Larson DE, et al. DNMT3A mutations in acute myeloid leukemia. N Engl J Med. 2010; 363(25):2424–33.10.1056/NEJMoa1005143 [PubMed: 21067377]
11. Yan XJ, Xu J, Gu ZH, Pan CM, Lu G, Shen Y, et al. Exome sequencing identifies somatic mutations of DNA methyltransferase gene DNMT3A in acute monocytic leukemia. Nat Genet. 2011; 43(4):309–15.10.1038/ng.788 [PubMed: 21399634]
12. Marcucci G, Metzeler KH, Schwind S, Becker H, Maharry K, Mrozek K, et al. Age-related prognostic impact of different types of DNMT3A mutations in adults with primary cytogenetically normal acute myeloid leukemia. Journal of clinical oncology : official journal of the American Society of Clinical Oncology. 2012; 30(7):742–50.10.1200/JCO.2011.39.2092 [PubMed: 22291079]
13. Ribeiro AF, Pratcorona M, Erpelinck-Verschueren C, Rockova V, Sanders M, Abbas S, et al. Mutant DNMT3A: a marker of poor prognosis in acute myeloid leukemia. Blood. 2012; 119(24): 5824–31.10.1182/blood-2011-07-367961 [PubMed: 22490330]
14. Im AP, Sehgal AR, Carroll MP, Smith BD, Tefferi A, Johnson DE, et al. DNMT3A and IDH mutations in acute myeloid leukemia and other myeloid malignancies: associations with prognosis and potential treatment strategies. Leukemia. 2014; 28(9):1774–83.10.1038/leu.2014.124 [PubMed: 24699305]
15. van Vlodrop IJ, Niessen HE, Derks S, Baldewijns MM, van Criekinge W, Herman JG, et al. Analysis of promoter CpG island hypermethylation in cancer: location, location, location! Clin Cancer Res. 2011; 17(13):4225–31.10.1158/1078-0432.CCR-10-3394 [PubMed: 21558408]
16. Shih AH, Abdel-Wahab O, Patel JP, Levine RL. The role of mutations in epigenetic regulators in myeloid malignancies. Nat Rev Cancer. 2012; 12(9):599–612.10.1038/nrc3343 [PubMed: 22898539]
17. Schoofs T, Berdel WE, Muller-Tidow C. Origins of aberrant DNA methylation in acute myeloid leukemia. Leukemia. 2014; 28(1):1–14.10.1038/leu.2013.242 [PubMed: 23958917]
18. Russler-Germain DA, Spencer DH, Young MA, Lamprecht TL, Miller CA, Fulton R, et al. The R882H DNMT3A mutation associated with AML dominantly inhibits wild-type DNMT3A by blocking its ability to form active tetramers. Cancer Cell. 2014; 25(4):442–54.10.1016/j.ccr.2014.02.010 [PubMed: 24656771]
19. Holz-Schietinger C, Matje DM, Reich NO. Mutations in DNA methyltransferase (DNMT3A) observed in acute myeloid leukemia patients disrupt processive methylation. J Biol Chem. 2012; 287(37):30941–51.10.1074/jbc.M112.366625 [PubMed: 22722925]
20. Okano M, Bell DW, Haber DA, Li E. DNA methyltransferases Dnmt3a and Dnmt3b are essential for de novo methylation and mammalian development. Cell. 1999; 99(3):247–57. [PubMed: 10555141]
21. Challen GA, Sun D, Jeong M, Luo M, Jelinek J, Berg JS, et al. Dnmt3a is essential for hematopoietic stem cell differentiation. Nat Genet. 2012; 44(1):23–31.10.1038/ng.1009 [PubMed: 22138693]
22. Nakao M, Yokota S, Iwai T, Kaneko H, Horiike S, Kashima K, et al. Internal tandem duplication of the flt3 gene found in acute myeloid leukemia. Leukemia. 1996; 10(12):1911–8. [PubMed: 8946930]
23. Kiyoi H, Towatari M, Yokota S, Hamaguchi M, Ohno R, Saito H, et al. Internal tandem duplication of the FLT3 gene is a novel modality of elongation mutation which causes constitutive activation of the product. Leukemia. 1998; 12(9):1333–7. [PubMed: 9737679]
24. Kiyoi H, Ohno R, Ueda R, Saito H, Naoe T. Mechanism of constitutive activation of FLT3 with internal tandem duplication in the juxtamembrane domain. Oncogene. 2002; 21(16):2555–63.10.1038/sj.onc.1205332 [PubMed: 11971190]
25. Mead AJ, Kharazi S, Atkinson D, Macaulay I, Pecquet C, Loughran S, et al. FLT3-ITDs instruct a myeloid differentiation and transformation bias in lymphomyeloid multipotent progenitors. Cell reports. 2013; 3(6):1766–76.10.1016/j.celrep.2013.04.031 [PubMed: 23727242]
26. Sexauer A, Perl A, Yang X, Borowitz M, Gocke C, Rajkhowa T, et al. Terminal myeloid differentiation in vivo is induced by FLT3 inhibition in FLT3/ITD AML. Blood. 2012; 120(20): 4205–14.10.1182/blood-2012-01-402545 [PubMed: 23012328]

27. Lee BH, Tothova Z, Levine RL, Anderson K, Buza-Vidas N, Cullen DE, et al. FLT3 mutations confer enhanced proliferation and survival properties to multipotent progenitors in a murine model of chronic myelomonocytic leukemia. Cancer Cell. 2007; 12(4):367–80.10.1016/j.ccr.2007.08.031 [PubMed: 17936561]

28. Hayakawa F, Towatari M, Kiyoi H, Tanimoto M, Kitamura T, Saito H, et al. Tandem-duplicated Flt3 constitutively activates STAT5 and MAP kinase and introduces autonomous cell growth in IL-3-dependent cell lines. Oncogene. 2000; 19(5):624–31.10.1038/sj.onc.1203354 [PubMed: 10698507]

29. Mizuki M, Fenski R, Halfter H, Matsumura I, Schmidt R, Muller C, et al. Flt3 mutations from patients with acute myeloid leukemia induce transformation of 32D cells mediated by the Ras and STAT5 pathways. Blood. 2000; 96(12):3907–14. [PubMed: 11090077]

30. Spiekermann K, Bagrintseva K, Schwab R, Schmieja K, Hiddemann W. Overexpression and constitutive activation of FLT3 induces STAT5 activation in primary acute myeloid leukemia blast cells. Clin Cancer Res. 2003; 9(6):2140–50. [PubMed: 12796379]

31. Fiskus W, Sharma S, Qi J, Shah B, Devaraj SG, Leveque C, et al. BET protein antagonist JQ1 is synergistically lethal with FLT3 tyrosine kinase inhibitor (TKI) and overcomes resistance to FLT3-TKI in AML cells expressing FLT-ITD. Mol Cancer Ther. 2014; 13(10):2315–27.10.1158/1535-7163.MCT-14-0258 [PubMed: 25053825]

32. Tickenbrock L, Schwable J, Wiedehage M, Steffen B, Sargin B, Choudhary C, et al. Flt3 tandem duplication mutations cooperate with Wnt signaling in leukemic signal transduction. Blood. 2005; 105(9):3699–706.10.1182/blood-2004-07-2924 [PubMed: 15650056]

33. Kelly LM, Liu Q, Kutok JL, Williams IR, Boulton CL, Gilliland DG. FLT3 internal tandem duplication mutations associated with human acute myeloid leukemias induce myeloproliferative disease in a murine bone marrow transplant model. Blood. 2002; 99(1):310–8. [PubMed: 11756186]

34. Lee BH, Williams IR, Anastasiadou E, Boulton CL, Joseph SW, Amaral SM, et al. FLT3 internal tandem duplication mutations induce myeloproliferative or lymphoid disease in a transgenic mouse model. Oncogene. 2005; 24(53):7882–92.10.1038/sj.onc.1208933 [PubMed: 16116483]

35. Zorko NA, Bernot KM, Whitman SP, Siebenaler RF, Ahmed EH, Marcucci GG, et al. Mll partial tandem duplication and Flt3 internal tandem duplication in a double knock-in mouse recapitulates features of counterpart human acute myeloid leukemias. Blood. 2012; 120(5):1130–6.10.1182/blood-2012-03-415067 [PubMed: 22674806]

36. Kogan SC, Ward JM, Anver MR, Berman JJ, Brayton C, Cardiff RD, et al. Bethesda proposals for classification of nonlymphoid hematopoietic neoplasms in mice. Blood. 2002; 100(1):238–45. [PubMed: 12070033]

37. Akalin A, Garrett-Bakelman FE, Kormaksson M, Busuttil J, Zhang L, Khrebtukova I, et al. Base-pair resolution DNA methylation sequencing reveals profoundly divergent epigenetic landscapes in acute myeloid leukemia. PLoS Genet. 2012; 8(6):e1002781.10.1371/journal.pgen.1002781 [PubMed: 22737091]

38. Figueroa ME, Abdel-Wahab O, Lu C, Ward PS, Patel J, Shih A, et al. Leukemic IDH1 and IDH2 mutations result in a hypermethylation phenotype, disrupt TET2 function, and impair hematopoietic differentiation. Cancer Cell. 2010; 18(6):553–67. Epub 2010/12/07. 10.1016/j.ccr.2010.11.015 [PubMed: 21130701]

39. Figueroa ME, Lugthart S, Li Y, Erpelinck-Verschueren C, Deng X, Christos PJ, et al. DNA methylation signatures identify biologically distinct subtypes in acute myeloid leukemia. Cancer Cell. 2010; 17(1):13–27. Epub 2010/01/12. 10.1016/j.ccr.2009.11.020 [PubMed: 20060365]

40. Challen GA, Sun D, Mayle A, Jeong M, Luo M, Rodriguez B, et al. Dnmt3a and dnmt3b have overlapping and distinct functions in hematopoietic stem cells. Cell stem cell. 2014; 15(3):350–64.10.1016/j.stem.2014.06.018 [PubMed: 25130491]

41. Mootha VK, Lindgren CM, Eriksson KF, Subramanian A, Sihag S, Lehar J, et al. PGC-1alpha-responsive genes involved in oxidative phosphorylation are coordinately downregulated in human diabetes. Nat Genet. 2003; 34(3):267–73. Epub 2003/06/17. 10.1038/ng1180 [PubMed: 12808457]

42. Subramanian A, Tamayo P, Mootha VK, Mukherjee S, Ebert BL, Gillette MA, et al. Gene set enrichment analysis: a knowledge-based approach for interpreting genome-wide expression

profiles. Proc Natl Acad Sci U S A. 2005; 102(43):15545–50.10.1073/pnas.0506580102 [PubMed: 16199517]

43. Reavie L, Della Gatta G, Crusio K, Aranda-Orgilles B, Buckley SM, Thompson B, et al. Regulation of hematopoietic stem cell differentiation by a single ubiquitin ligase-substrate complex. Nat Immunol. 2010; 11(3):207–15.10.1038/ni.1839 [PubMed: 20081848]
44. Emig D, Salomonis N, Baumbach J, Lengauer T, Conklin BR, Albrecht M. AltAnalyze and DomainGraph: analyzing and visualizing exon expression data. Nucleic Acids Res. 2010; 38(Web Server issue):W755–62.10.1093/nar/gkq405 [PubMed: 20513647]
45. Zambon AC, Gaj S, Ho I, Hanspers K, Vranizan K, Evelo CT, et al. GO-Elite: a flexible solution for pathway and ontology over-representation. Bioinformatics. 2012; 28(16):2209–10.10.1093/bioinformatics/bts366 [PubMed: 22743224]
46. Visvader JE, Lindeman GJ. Cancer stem cells: current status and evolving complexities. Cell stem cell. 2012; 10(6):717–28.10.1016/j.stem.2012.05.007 [PubMed: 22704512]
47. Bourdeau A, Trop S, Doody KM, Dumont DJ, Tremblay ML. Inhibition of T cell protein tyrosine phosphatase enhances interleukin-18-dependent hematopoietic stem cell expansion. Stem Cells. 2013; 31(2):293–304.10.1002/stem.1276 [PubMed: 23135963]
48. Rau R, Magoon D, Greenblatt S, Li L, Annesley C, Duffield AS, et al. NPMc+ cooperates with Flt3/ITD mutations to cause acute leukemia recapitulating human disease. Experimental hematology. 2014; 42(2):101–13. e5.10.1016/j.exphem.2013.10.005 [PubMed: 24184354]
49. Guryanova OA, Lieu YK, Garrett-Bakelman FE, Spitzer B, Glass JL, Shank K, et al. Dnmt3a regulates myeloproliferation and liver-specific expansion of hematopoietic stem and progenitor cells. Leukemia. 2015 Epub 2015/12/30. 10.1038/leu.2015.358
50. Chang YI, You X, Kong G, Ranheim EA, Wang J, Du J, et al. Loss of Dnmt3a and endogenous Kras(G12D/+) cooperate to regulate hematopoietic stem and progenitor cell functions in leukemogenesis. Leukemia. 2015; 29(9):1847–56.10.1038/leu.2015.85 [PubMed: 25801914]
51. Schlenk RF, Kayser S, Bullinger L, Kobbe G, Casper J, Ringhoffer M, et al. Differential impact of allelic ratio and insertion site in FLT3-ITD-positive AML with respect to allogeneic transplantation. Blood. 2014; 124(23):3441–9. Epub 2014/10/02. 10.1182/blood-2014-05-578070 [PubMed: 25270908]
52. Kim MS, Yoon SK, Bollig F, Kitagaki J, Hur W, Whye NJ, et al. A novel Wilms tumor 1 (WT1) target gene negatively regulates the WNT signaling pathway. J Biol Chem. 2010; 285(19):14585–93. Epub 2010/03/12. 10.1074/jbc.M109.094334 [PubMed: 20220130]
53. Andersson T, Sodersten E, Duckworth JK, Cascante A, Fritz N, Sacchetti P, et al. CXXC5 is a novel BMP4-regulated modulator of Wnt signaling in neural stem cells. J Biol Chem. 2009; 284(6):3672–81. Epub 2008/11/13. 10.1074/jbc.M808119200 [PubMed: 19001364]
54. Liu N, Wang M, Deng W, Schmidt CS, Qin W, Leonhardt H, et al. Intrinsic and extrinsic connections of Tet3 dioxygenase with CXXC zinc finger modules. PLoS One. 2013; 8(5):e62755. Epub 2013/05/22. 10.1371/journal.pone.0062755 [PubMed: 23690950]
55. Treppendahl MB, Mollgard L, Hellstrom-Lindberg E, Cloos P, Gronbaek K. Downregulation but lack of promoter hypermethylation or somatic mutations of the potential tumor suppressor CXXC5 in MDS and AML with deletion 5q. European journal of haematology. 2013; 90(3):259–60. Epub 2012/11/30. 10.1111/ejh.12045 [PubMed: 23190153]
56. Kuhnl A, Valk PJ, Sanders MA, Ivey A, Hills RK, Mills KI, et al. Downregulation of the Wnt inhibitor CXXC5 predicts a better prognosis in acute myeloid leukemia. Blood. 2015; 125(19):2985–94. Epub 2015/03/26. 10.1182/blood-2014-12-613703 [PubMed: 25805812]
57. Astori A, Fredly H, Aloysius TA, Bullinger L, Mansat-De Mas V, de la Grange P, et al. CXXC5 (retinoid-inducible nuclear factor, RINF) is a potential therapeutic target in high-risk human acute myeloid leukemia. Oncotarget. 2013; 4(9):1438–48. Epub 2013/08/31. 10.18632/oncotarget.1195 [PubMed: 23988457]
58. Marastoni S, Andreuzzi E, Paulitti A, Colladel R, Pellicani R, Todaro F, et al. EMILIN2 down-modulates the Wnt signalling pathway and suppresses breast cancer cell growth and migration. The Journal of pathology. 2014; 232(4):391–404. Epub 2014/01/01. 10.1002/path.4316 [PubMed: 24374807]

59. Genovese G, Kahler AK, Handsaker RE, Lindberg J, Rose SA, Bakhoum SF, et al. Clonal hematopoiesis and blood-cancer risk inferred from blood DNA sequence. N Engl J Med. 2014; 371(26):2477–87.10.1056/NEJMoa1409405 [PubMed: 25426838]
60. Xie M, Lu C, Wang J, McLellan MD, Johnson KJ, Wendl MC, et al. Age-related mutations associated with clonal hematopoietic expansion and malignancies. Nat Med. 2014; 20(12):1472–8. Epub 2014/10/20. 10.1038/nm.3733 [PubMed: 25326804]
61. Kaneda M, Okano M, Hata K, Sado T, Tsujimoto N, Li E, et al. Essential role for de novo DNA methyltransferase Dnmt3a in paternal and maternal imprinting. Nature. 2004; 429(6994):900–3.10.1038/nature02633 [PubMed: 15215868]
62. Kuhn R, Schwenk F, Aguet M, Rajewsky K. Inducible gene targeting in mice. Science. 1995; 269(5229):1427–9. [PubMed: 7660125]
63. Le Beau MM, Bitts S, Davis EM, Kogan SC. Recurring chromosomal abnormalities in leukemia in PML-RARA transgenic mice parallel human acute promyelocytic leukemia. Blood. 2002; 99(8): 2985–91. [PubMed: 11929790]
64. Meyer SE, Zinser GM, Stuart WD, Pathrose P, Waltz SE. The Ron receptor tyrosine kinase negatively regulates mammary gland branching morphogenesis. Developmental Biology. 2009; 333(1):173–85.10.1016/j.ydbio.2009.06.028 [PubMed: 19576199]
65. Kim D, Pertea G, Trapnell C, Pimentel H, Kelley R, Salzberg SL. TopHat2: accurate alignment of transcriptomes in the presence of insertions, deletions and gene fusions. Genome Biol. 2013; 14(4):R36.10.1186/gb-2013-14-4-r36 [PubMed: 23618408]
66. Trapnell C, Pachter L, Salzberg SL. TopHat: discovering splice junctions with RNA-Seq. Bioinformatics. 2009; 25(9):1105–11.10.1093/bioinformatics/btp120 [PubMed: 19289445]
67. Li B, Dewey CN. RSEM: accurate transcript quantification from RNA-Seq data with or without a reference genome. BMC Bioinformatics. 2011; 12:323.10.1186/1471-2105-12-323 [PubMed: 21816040]
68. Verhaak RG, Wouters BJ, Erpelinck CA, Abbas S, Beverloo HB, Lugthart S, et al. Prediction of molecular subtypes in acute myeloid leukemia based on gene expression profiling. Haematologica. 2009; 94(1):131–4. Epub 2008/10/08. haematol.13299 [pii]. 10.3324/haematol.13299 [PubMed: 18838472]
69. Shih AH, Jiang Y, Meydan C, Shank K, Pandey S, Barreyro L, et al. Mutational cooperativity linked to combinatorial epigenetic gain of function in acute myeloid leukemia. Cancer Cell. 2015; 27(4):502–15. Epub 2015/04/16. 10.1016/j.ccell.2015.03.009 [PubMed: 25873173]
70. Garrett-Bakelman FE, Sheridan CK, Kacmarczyk TJ, Ishii J, Betel D, Alonso A, et al. Enhanced reduced representation bisulfite sequencing for assessment of DNA methylation at base pair resolution. J Vis Exp. 2015; (96):e52246.10.3791/52246 [PubMed: 25742437]
71. Krueger F, Andrews SR. Bismark: a flexible aligner and methylation caller for Bisulfite-Seq applications. Bioinformatics. 2011; 27(11):1571–2.10.1093/bioinformatics/btr167 [PubMed: 21493656]
72. Park Y, Figueroa ME, Rozek LS, Sartor MA. MethylSig: a whole genome DNA methylation analysis pipeline. Bioinformatics. 2014; 30(17):2414–22.10.1093/bioinformatics/btu339 [PubMed: 24836530]
73. Akalin A, Kormaksson M, Li S, Garrett-Bakelman FE, Figueroa ME, Melnick A, et al. methylKit: a comprehensive R package for the analysis of genome-wide DNA methylation profiles. Genome Biol. 2012; 13(10):R87.10.1186/gb-2012-13-10-r87 [PubMed: 23034086]
74. Meldi K, Qin T, Buchi F, Droin N, Sotzen J, Micol JB, et al. Specific molecular signatures predict decitabine response in chronic myelomonocytic leukemia. J Clin Invest. 2015; 125(5):1857–72.10.1172/JCI78752 [PubMed: 25822018]
75. Naviaux RK, Costanzi E, Haas M, Verma IM. The pCL vector system: rapid production of helper-free, high-titer, recombinant retroviruses. J Virol. 1996; 70(8):5701–5. [PubMed: 8764092]
76. Naldini L, Blomer U, Gage FH, Trono D, Verma IM. Efficient transfer, integration, and sustained long-term expression of the transgene in adult rat brains injected with a lentiviral vector. Proc Natl Acad Sci U S A. 1996; 93(21):11382–8. [PubMed: 8876144]
77. Burns JC, Friedmann T, Driever W, Burrascano M, Yee JK. Vesicular stomatitis virus G glycoprotein pseudotyped retroviral vectors: concentration to very high titer and efficient gene

transfer into mammalian and nonmammalian cells. Proc Natl Acad Sci U S A. 1993; 90(17):8033–7. [PubMed: 8396259]

Significance

Dnmt3a haploinsufficiency results in reversible epigenetic alterations that transform Flt3-ITD mutant myeloproliferative neoplasm into acute myeloid leukemia.

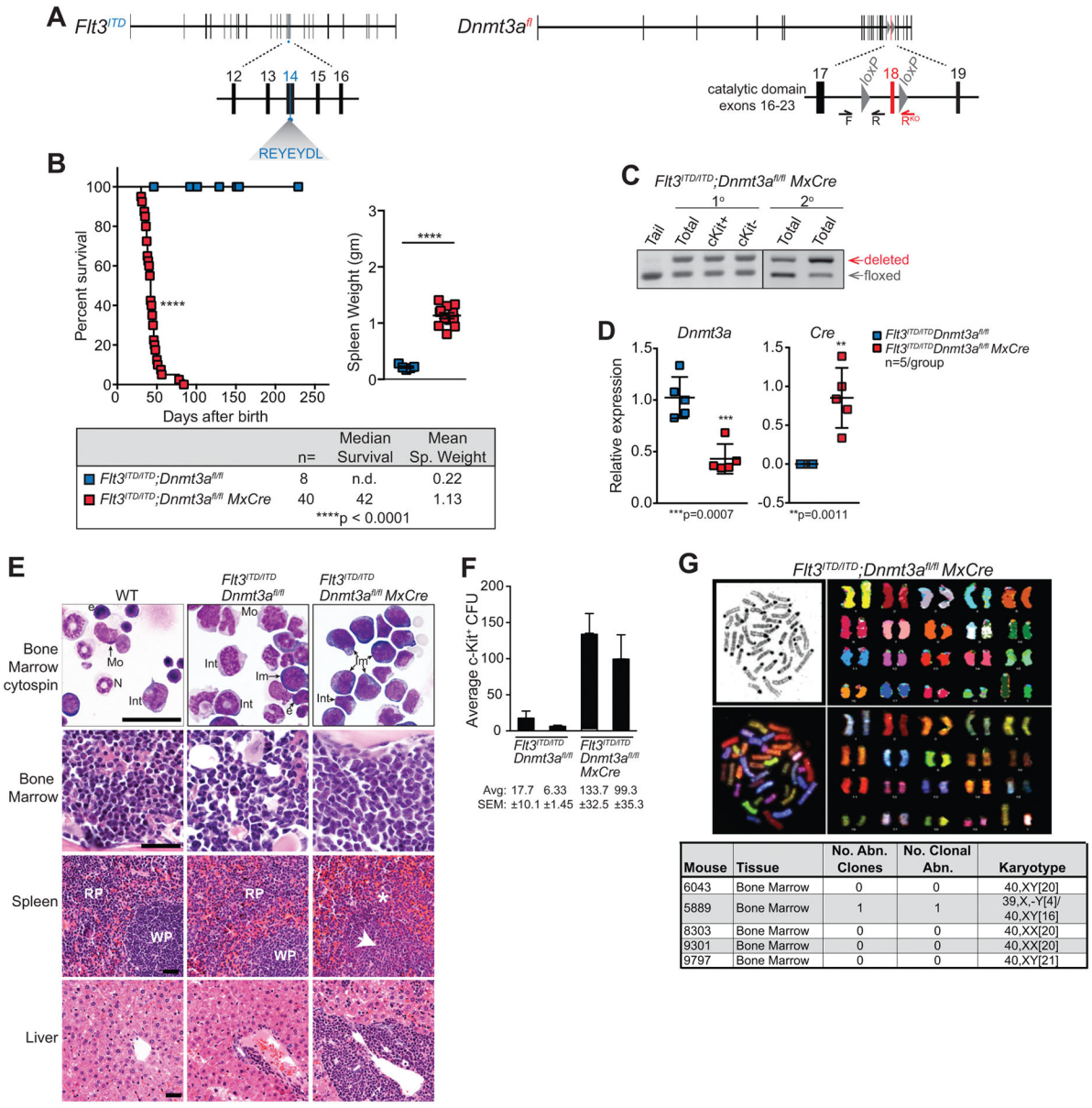

Figure 1. A rapid, spontaneous, and fully penetrant model of cytogenetically normal AML utilizing *Flt3*^{ITD} and *Dnmt3a* haploinsufficiency

A, Schematic of mouse alleles with constitutive Flt3-ITD knock-in (*Flt3*^{ITD}) and *Dnmt3a* exon 18 flanked by *loxP* sites (*Dnmt3a*^{fl}). **B,** Kaplan-Meier survival curves (left) and spleen weights (right) of *Flt3*$^{ITD/ITD}$*;Dnmt3a*$^{fl/fl}$ mice without (blue squares) and with Mx1-Cre (*MxCre*) (red squares). Table beneath summarizes the number of animals, median survivals, and mean spleen weights of mice in panel **B.** Significant differences in survival were evaluated by Log-rank (Mantel-Cox) test and by unpaired parametric t-test. **C,** Representative semi-quantitative PCR detection of *Dnmt3a loxP* sites from tail or c-Kit^{+} fractionated leukemic splenocyte genomic DNA from primary and secondary transplant recipient *Flt3*$^{ITD/ITD}$*;Dnmt3a*$^{fl/fl}$ *MxCre* mice ("deleted" indicates deletion of a single floxed *Dnmt3a* exon 18; "floxed" indicates no recombination). Additional 5 independent

Flt3$^{ITD/ITD}$;*Dnmt3a*$^{fl/fl}$ *MxCre* showed similar results (see also Supplementary Fig. 1C). **D,** RT-qPCR for *Dnmt3a* (left) and *Cre* (right) expression in c-Kit^{+} leukemic splenocytes from individual *Flt3*$^{ITD/ITD}$;*Dnmt3a*$^{fl/fl}$ *MxCre* and *Flt3*$^{ITD/ITD}$;*Dnmt3a*$^{fl/fl}$ mice (n=5/group). Significance was determined by unpaired parametric t-test. **E,** Representative Wright Giemsa stained bone marrow cytospins and H&E stained bone marrow, spleen, and liver from wild-type (WT), *Flt3*$^{ITD/ITD}$;*Dnmt3a*$^{fl/fl}$, and *Flt3*$^{ITD/ITD}$;*Dnmt3a*$^{fl/fl}$ *MxCre* mice. Top panels cytospins: Normal WT marrow cytospins shows a mixture of erythroid (e) and myeloid elements including neutrophilic (N), intermediate (Int) and monocytic (Mo) (lymphocytes present in other microscopic fields). *Flt3*$^{ITD/ITD}$;*Dnmt3a*$^{fl/fl}$ marrow is predominantly myelomonocytic, with increased monocytes, increased intermediate myeloid forms and few immature (Im) forms *Flt3*$^{ITD/ITD}$;*Dnmt3a*$^{fl/fl}$ *MxCre* marrow has numerous immature forms and intermediate myeloid forms. Second row panels marrow H&E show bone marrow histology consistent with the cellular constituents seen in cytospins; note numerous dark nuclei of erythroids in WT marrow, mixture of maturing myelomonocytic elements in *Flt3*$^{ITD/ITD}$;*Dnmt3a*$^{fl/fl}$, and predominance of less mature forms (including immature forms/blasts) in *Flt3*$^{ITD/ITD}$;*Dnmt3a*$^{fl/fl}$ *MxCre.* Third row panels spleen H&E: In WT spleen, there is a clearly demarcated lymphoid area of white pulp (WP), and red pulp (RP) is predominantly erythroid. In *Flt3*$^{ITD/ITD}$;*Dnmt3a*$^{fl/fl}$ spleen, there is some alteration of lymphocyte morphology (more cytoplasm, including an increase in lymphocytes with a marginal zone morphology) in the white pulp and the red pulp is expanded with mixed myeloid hyperplasia (erythroid, megakaryocytes, neutrophils, and monocytic cells). In *Flt3*$^{ITD/ITD}$;*Dnmt3a*$^{fl/fl}$ *MxCre* spleen there is a loss of white pulp. The area indicated by white arrow is not lymphoid but rather is composed predominantly of myelomonocytic cells including immature elements. The larger areas of red pulp (*) are expanded with mixed myeloid hyperplasia (erythroid, megakaryocytes, neutrophils, monocytic cells). **F,** Average ±SEM number of colonies arising from c-Kit^{+} splenocytes from *Flt3*$^{ITD/ITD}$;*Dnmt3a*$^{fl/fl}$ and *Flt3*$^{ITD/ITD}$;*Dnmt3a*$^{fl/fl}$ *MxCre* mice after 7 days in methylcellulose. Each bar represents individual mice (n=2/group). **G,** Spectral karyotyping analysis of a representative *Flt3*$^{ITD/ITD}$;*Dnmt3a*$^{fl/fl}$ *MxCre* bone marrow illustrating the inverted image of the DAPI-stained metaphase cell (upper left), the spectral image (lower left), spectral karyotype (lower right), and the karyotype from the classified image (upper right). The karyotype was 40,XY. Below is a table summarizing the karyotypes found in individual leukemic mice by spectral karyotyping (n=5).

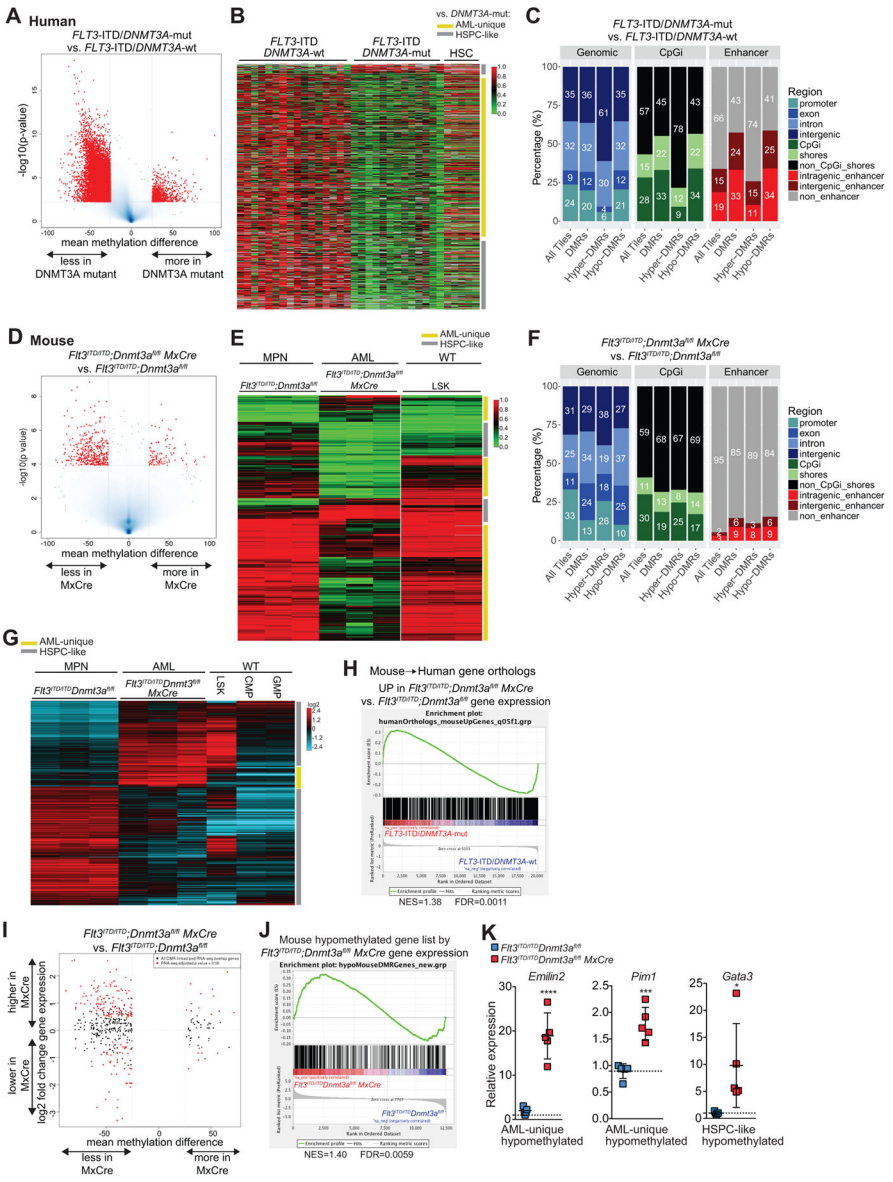

Figure 2. Genome-wide DNA hypo-methylation associated with *DNMT3A* mutation in murine and human *FLT3*-ITD AML

Human: **A–C,** Volcano plot (**A**) representation of mean methylation difference (x-axis) versus statistical significance (y-axis). Red dots designate significantly hypo- and hyper-methylated regions in *FLT3*-ITD/*DNMT3A*-mut AML patients compared to patients with *FLT3*-ITD alone. **B,** Heatmap representation of differentially methylated regions in *FLT3*-ITD/*DNMT3A*-mut AML compared to *FLT3*-ITD/*DNMT3A*-wt AML. Corresponding methylation levels are also shown in normal human bone marrow hematopoietic stem cells (HSC) for normal baseline comparison. **C,** Proportion of all measured CpGs by ERRBS (all tiles) and differentially methylated in *FLT3*-ITD/*DNMT3A*-mut versus *FLT3*-ITD/*DNMT3A*-wt AML (DMRs, hypermethylated, and hypomethylated) in genomic, CpG island (CpGi), and enhancer regions. Murine (n=3 mice/group): **D–F,** Volcano plot (**D**) representation of mean methylation difference (x-axis) versus statistical significance (y-

axis). Red dots designate significantly differentially methylated regions in *Flt3*$^{ITD/ITD}$*;Dnmt3a*$^{fl/fl}$ *MxCre* AML compared to *Flt3*$^{ITD/ITD}$*;Dnmt3a*$^{fl/fl}$ MPN. **E,** Heatmap representation of differentially methylated regions in *Flt3*$^{ITD/ITD}$*;Dnmt3a*$^{fl/fl}$ *MxCre* AML compared to *Flt3*$^{ITD/ITD}$*;Dnmt3a*$^{fl/fl}$ MPN. Corresponding methylation levels are also shown in WT murine Lin^{-}Sca-1^{+}c-Kit^{+} (LSK) as a normal baseline comparison. HSPC-like genes share similar methylation patterns with WT LSK (indicated by gray sidebars) and AML-unique regions are differentially methylated from both MPN and WT LSK (indicated by gold sidebars). **F,** Proportion of differentially methylated genomic, CpGi, and enhancer regions in all measured CpGs (all tiles) and DMRs (hypermethylated and hypomethylated) in *Flt3*$^{ITD/ITD}$*;Dnmt3a*$^{fl/fl}$ *MxCre* AML compared to *Flt3*$^{ITD/ITD}$*;Dnmt3a*$^{fl/fl}$ MPN murine models. **G,** Gene expression: Hierarchical clustering of significantly differentially expressed genes in *Flt3*$^{ITD/ITD}$*;Dnmt3a*$^{fl/fl}$ *MxCre* AML compared to *Flt3*$^{ITD/ITD}$*;Dnmt3a*$^{fl/fl}$ MPN. Gene expression is also shown for WT LSK, common myeloid progenitors (CMP), and granulocyte-monocyte progenitors (GMP) murine bone marrow cells as normal baseline comparison. “HSPC-like” genes are expressed in AML and LSK but not in CMP, GMP or the MPN. “AML-unique” genes are differentially expressed in AML compared to all other samples. **H,** GSEA: Genes upregulated in murine AML versus MPN were ranked according to descending gene expression in human *FLT3*-ITD/*DNMT3A*-mut AML versus *FLT3*-ITD/*DNMT3A*-wt AML. **I,** Dot plot representation of mean methylation difference for all differentially methylated genes in c-Kit^{+} *Flt3*$^{ITD/ITD}$*;Dnmt3a*$^{fl/fl}$ *MxCre* AML compared to *Flt3*$^{ITD/ITD}$*;Dnmt3a*$^{fl/fl}$ MPN (x-axis), versus their corresponding gene expression fold change (y-axis) (n=3 mice/group). Genes whose gene expression changes overlapped with changes in methylation are highlighted in red. **J,** GSEA: Genes corresponding to hypo-methylated regions in murine *Flt3*$^{ITD/ITD}$*;Dnmt3a*$^{fl/fl}$ *MxCre* AML (compared to MPN) were ranked according to descending gene expression in murine AML versus MPN. **K,** RT-qPCR validation of representative genes from AML-unique and HSPC-like groups in panel **G** that were hypo-methylated in murine c-Kit^{+} splenocytes from *Flt3*$^{ITD/ITD}$*;Dnmt3a*$^{fl/fl}$ *MxCre* AML (red boxes) versus *Flt3*$^{ITD/ITD}$*;Dnmt3a*$^{fl/fl}$ MPN (blue boxes) (n=5 mice/group). Statistical significance was evaluated by unpaired parametric t-test.

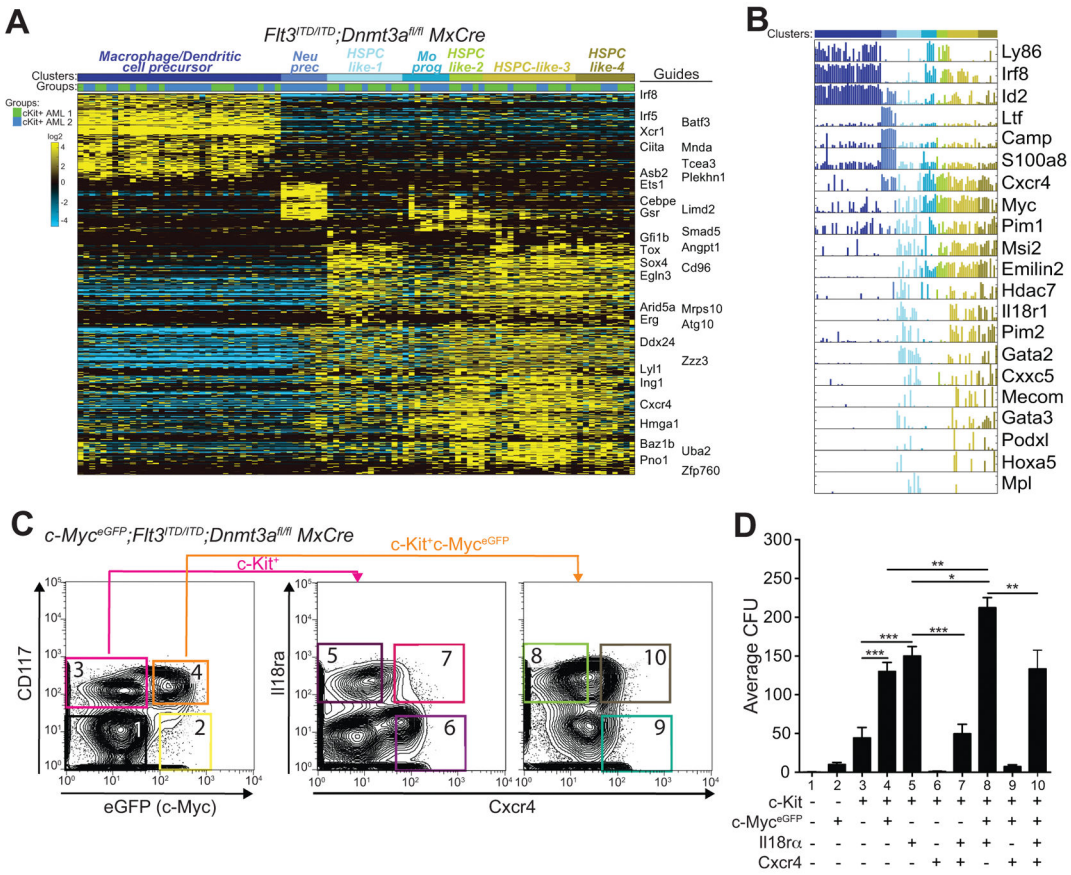

Figure 3. Single-cell RNA-Seq to determine the cellular structure of the *Flt3$^{ITD/ITD}$;Dnmt3a$^{fl/fl}$ MxCre* AML model

Ninety-six scRNA-Seq libraries were constructed from the c-Kit^{+} leukemic splenocytes of 2 independent *Flt3$^{ITD/ITD}$;Dnmt3a$^{fl/fl}$ MxCre* AML. **A,** Iterative Clustering and Guide-gene Selection (ICGS) HOPACH clustering of gene expression resolves AML subpopulations (clusters: Macrophage Dendritic cell precursor, Neutrophil precursor, HSPC-like-1, Monocyte progenitor, HSPC-like-2, HSPC-like-3, HSPC-like-4), based on gene ontology enrichment analysis (GO-Elite) and literature associations. Genes listed to the right represent the ICGS-selected guide genes (the most intracorrelated gene) within each of these clusters. **B,** Column plots demonstrate amplitude (transcripts per million, TPM) and incidence of selected gene expression in the same ICGS-derived cell ordering as in panel **A. C,** Given the enrichment for *c-Myc, IL18r1,* and *Cxcr4* expression in the HSPC-like subpopulations in panel **B**, c-Myc^{eGFP} fusion-protein knock-in alleles were bred into the *Flt3$^{ITD/ITD}$;Dnmt3a$^{fl/fl}$ MxCre* AML model and antibodies to the latter proteins were used to analyze c-Kit^{+} *Flt3$^{ITD/ITD}$;Dnmt3a$^{fl/fl}$ MxCre* AML splenocytes. Representative flow plots illustrating the gates for sorting AML subpopulations are shown. Each sorted AML subpopulation (numbered 1–10) were examined for clonogenicity in methylcellulose colony forming assays. **D,** A representative experiment is shown depicting the average ±SEM number of colonies formed for each of the gated subpopulations in panel **C** after 7 days in methylcellulose. CFU assays were repeated three times with independent *c-Myc^{eGFP};Flt3$^{ITD/ITD}$;Dnmt3a$^{fl/fl}$ MxCre* AML, and produced similar results. Significant

differences in colony numbers were evaluated by one-way ANOVA Tukey's multiple comparisons test.

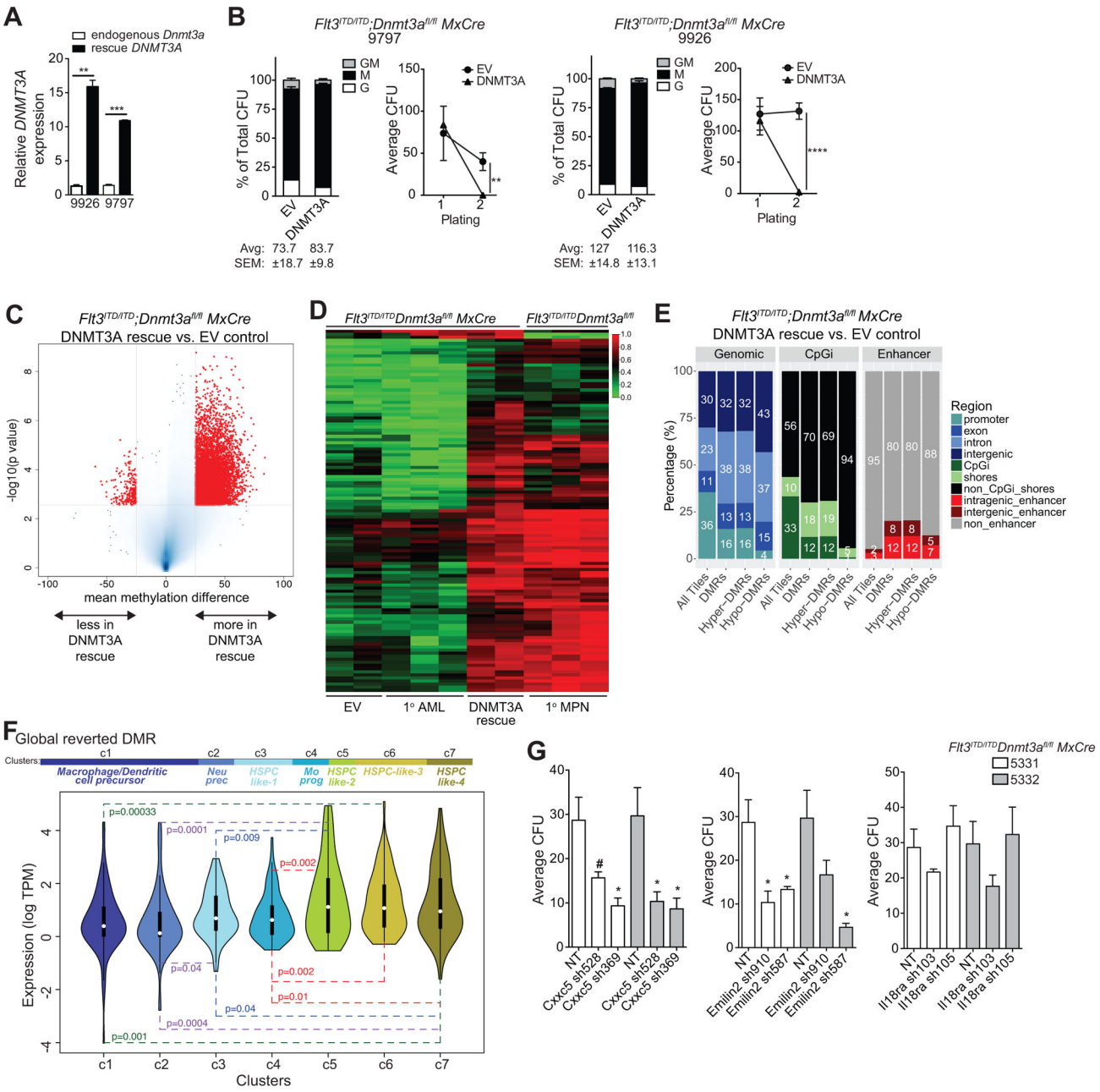

Figure 4. Rescuing DNMT3A expression is associated with reversion of DNA hypo-methylation and loss of clonogenicity

c-Kit^{+} AML splenocytes from two different donor *Flt3*$^{ITD/ITD}$*;Dnmt3a*$^{fl/fl}$ *MxCre* AML mice were transduced with wild-type DNMT3A (DNMT3A) or empty vector (EV) control to rescue Dnmt3a expression. **A,** Average ±SEM of endogenous *Dnmt3a* and rescue *DNMT3A* expression in WT DNMT3A transduced *Flt3*$^{ITD/ITD}$*;Dnmt3a*$^{fl/fl}$ *MxCre* AML CFU relative to endogenous *Dnmt3a* in matched EV control (*Sdha* served as control). Significance was evaluated by unpaired parametric t-test. **B,** Average ±SEM relative proportions of granulocyte (CFU-G), monocyte (CFU-M) and mixed (CFU-GM) colonies formed after 7 days in methylcellulose (left stacked bar graphs) and average ±SEM number

of colonies in two serial platings (right line graphs) with DNMT3A rescue or EV control *Flt3*$^{ITD/ITD}$*;Dnmt3a*$^{fl/fl}$ *MxCre* AML cells. Significant reduction in CFU formed by DNMT3A rescued cells compared to EV control was determined by unpaired parametric t-test. Two independent mice are shown; averages are technical replicates per mouse. The experiment was repeated twice with similar results. **C,** Volcano plot representation of mean methylation difference (x-axis) vs. statistical significance (y-axis). Red dots designate significantly differentially methylated regions in *DNMT3A*-rescued *Flt3*$^{ITD/ITD}$*;Dnmt3a*$^{fl/fl}$ *MxCre* AML versus EV control from panel **B. D,** Heatmap representation of differentially methylated regions in DNMT3A-rescued versus EV control *Flt3*$^{ITD/ITD}$*;Dnmt3a*$^{fl/fl}$ *MxCre* AML from panel **B.** Corresponding levels of methylation for those regions are also shown in the primary *Flt3*$^{ITD/ITD}$*;Dnmt3a*$^{fl/fl}$ MPN (1°MPN) and *Flt3*$^{ITD/ITD}$*;Dnmt3a*$^{fl/fl}$ AML (1°AML). **E,** Proportion of differentially methylated genomic, CpGi, and enhancer regions in all measured CpGs (all tiles) and DMRs (hypermethylated and hypomethylated) in DNMT3A-rescued compared to EV control transduced *Flt3*$^{ITD/ITD}$*;Dnmt3a*$^{fl/fl}$ *MxCre* AML from panel **B. F,** Violin plots represent the expression of genes associated with remethylated DMRs in panel **D,** within the ICGS clusters from Fig. 3A. G, Average ±SEM number of colonies from c-Kit^{+} AML splenocytes from two different donor *Flt3*$^{ITD/ITD}$*;Dnmt3a*$^{fl/fl}$ *MxCre* AML mice (two independent mice denoted by white or gray bars) transduced with *Cxxc5*, *Emilin2*, *Il18r1* shRNA or non-targeting (NT) control. Significant reduction in CFU formed by *Cxxc5* and *Emilin2* knockdown AML cells compared to NT control was determined by unpaired parametric t-test (#p=0.07, *p<0.05). Two independent mice are shown; averages are technical replicates per mouse.